Generation and attenuation of variability in a bacterial signaling network revealed by single-cell FRET

J.M. Keegstra[1]**, K. Kamino**[1]**, F. Anquez §**[1]**, M.D. Lazova**[1]**, T. Emonet**[2]**, T.S. Shimizu**[1]

*For correspondence:
shimizu@amolf.nl (TSS)

Present address: §Laboratoire de Physique des Lasers, Atomes et Molécules, UMR CNRS 8523, Université Lille 1, France

[1]AMOLF Institute, Science Park 104, 1098XG Amsterdam, the Netherlands; [2]Department of Molecular, Cellular and Developmental Biology and Department of Physics, Yale University, New Haven CT, USA

Abstract   We present *in vivo* single-cell FRET measurements in the *Escherichia coli* chemotaxis system that reveal pervasive signaling variability, both across cells in isogenic populations and within individual cells over time. We quantify cell-to-cell variability of adaptation, ligand response, as well as steady-state output level, and analyze the role of network design in shaping this diversity from gene expression noise. In the absence of changes in gene expression, we find that single cells demonstrate strong temporal fluctuations. We provide evidence that such signaling noise can arise from at least two sources: (i) stochastic activities of adaptation enzymes, and (ii) receptor-kinase dynamics in the absence of adaptation. We demonstrate that under certain conditions, (ii) can generate giant fluctuations that drive signaling activity of the entire cell into a stochastic two-state switching regime. Our findings underscore the importance of molecular noise, arising not only in gene expression but also in protein networks.

Introduction

Cellular physiology is deeply shaped by molecular fluctuations, resulting in phenotypic variability that can be both detrimental and beneficial (*Rao et al., 2002*). One of the most important and well-studied sources of intracellular fluctuations is stochastic gene expression (*Elowitz et al., 2002*; *Eldar and Elowitz, 2010*; *Raj and Van Oudenaarden, 2008*), which can generate substantial cell-to-cell variability in protein levels within isogenic populations under invariant environmental conditions. Such heterogeneity in protein counts are readily measurable by fluorescent-protein reporters (*Elowitz et al., 2002*; *Ozbudak et al., 2002*) , but mechanistically tracing the consequences of such molecular noise to the level of complex cellular phenotypes such as signaling and motility remains a significant challenge, in part due to the multitude of interactions between gene products, but also because each of those interactions can, in principle, become an additional source of noise. In this paper, we study how multiple sources of molecular noise, arising in both gene expression and protein-protein interactions, affect performance of the *E. coli* chemotaxis network, a canonical signaling pathway.

In bacteria, gene-expression noise tends to manifest itself as stable cell-to-cell differences in phenotypes that persist over the cell's generation time, because typical protein lifetimes are longer than the cell cycle (*Li et al., 2014*). The architecture of signaling networks can have a profound influence on their sensitivity to such noise-induced differences in protein levels, and it has been shown that the design of the *E. coli* chemotaxis network confers robustness of a number of signaling parameters, such as precision of adaptation, against variability in gene expression (*Barkai and Leibler, 1997*; *Kollmann et al., 2005*). On the other hand, cell-to-cell differences in behavior can also be advantageous for isogenic populations under uncertain and/or time-varying environments, and it has been argued that the manner in which the chemotaxis network filters gene expression noise to shape phenotype distributions could be under selective pressure (*Frankel et al., 2014*; *Waite et al., 2016*).

In principle, molecular noise arising in processes other than gene expression, such as protein-protein interactions within signaling pathways, can also contribute to cellular variability. However, such noise sources tend to be harder to study experimentally because, in contrast to gene-expression noise, which can be characterized by measuring fluorescent reporter levels (*Elowitz et al., 2002*; *Raser and O'Shea, 2004*), requirements for *in vivo* measurements of protein-protein interactions tend to be more demanding and no generically applicable strategies exist. The *E. coli* chemotaxis system provides a compelling experimental paradigm for addressing protein-signaling noise, because a powerful technique for *in vivo* measurements of protein signaling, based on Förster resonance energy transfer (FRET), has been successfully developed (*Sourjik and Berg, 2002b*; *Sourjik et al., 2007*).

The chemotaxis network controls the motile behavior of *E. coli*, a run-and-tumble random

57 walk that is biased by the signaling network to achieve net migrations toward favorable directions.
58 The molecular mechanisms underlying this pathway have been studied extensively (for recent
59 reviews, see refs. *Wadhams and Armitage* (*2004*); *Tu* (*2013*); *Parkinson et al.* (*2015*)). In brief,
60 transmembrane chemoreceptors bind to ligand molecules, inhibiting the autophosphorylation of a
61 central kinase, CheA. When active, CheA transfers its phosphate to CheY to form CheY-P. Meanwhile,
62 the phosphatase CheZ degrades CheY-P to limit the signal lifetime. CheY-P binds to a flagellar
63 motor, which in turn increases the chance of the motor to turn clockwise, leading to a tumble.
64 An adaptation module consisting of the enzymes CheR and CheB implements negative integral
65 feedback by tuning the sensitivity of the chemoreceptors via reversible covalent modifications that
66 restore the kinase activity (and CheY-P level).

67 Despite its relative simplicity, this pathway exhibits many interesting network-level functionalities,
68 such as cooperative signal amplification (*Segall et al., 1986*; *Sourjik and Berg, 2002b*; *Bray et al.,*
69 *1998*), sensory adaptation (*Barkai and Leibler, 1997*; *Alon et al., 1999*) and fold-change detection
70 (*Mesibov et al., 1973*; *Lazova et al., 2011*), and FRET microscopy has proven extremely powerful in
71 characterizing such signal processing of the chemotaxis pathway, especially in *E. coli* (*Sourjik and*
72 *Berg, 2002b*, *2004*; *Shimizu et al., 2010*; *Oleksiuk et al., 2011*), but also in Salmonella (*Lazova et al.,*
73 *2012*) and *B. subtilis* (*Yang et al., 2015*). It has been implemented in various ways (*Sourjik and Berg,*
74 *2002b*,a; *Shimizu et al., 2006*; *Kentner and Sourjik, 2009*), but most commonly by using CFP and YFP
75 as the FRET donor-acceptor pair, fused to CheY and CheZ, respectively. To date, however, nearly all
76 applications of FRET in the bacterial chemotaxis system have been population-level measurements
77 in which signals from hundreds to thousands of cells are integrated to achieve a high signal-to-noise
78 ratio. A pioneering study applied FRET at the single-cell level to study spatial heterogeneities in
79 CheY-CheZ interactions (*Vaknin and Berg, 2004*), but those measurements were limited to relatively
80 short times due to phototoxicity and bleaching.

81 By exploring a range of fluorescent proteins as FRET pairs, and improving measurement pro-
82 tocols, we have developed a robust method for single-cell FRET measurements of chemotactic
83 signaling dynamics in single bacteria over extended times. The data reveal extensive cell-to-cell
84 variability, as well as temporal fluctuations that are masked in population-level FRET measure-
85 ments. In contrast to previous single-cell experiments that relied on measurements of motor
86 output or swimming behavior (*Berg and Brown, 1972*; *Spudich and Koshland, 1976*; *Segall et al.,*
87 *1986*; *Korobkova et al., 2004*; *Park et al., 2010*; *Masson et al., 2012*), FRET alleviates the need to
88 make indirect inferences about intracellular molecular interactions through the highly noisy 2-state
89 switching of the flagellar motor, whose response function can vary over time due to adaptive
90 remodeling (*Yuan et al., 2012*). In a typical experiment, we are able to obtain dozens of (up to
91 ~100) single-cell FRET time series simultaneously, to efficiently collect statistics of phenotypic and
92 temporal variability.

Results

Single-cell FRET reveals pervasive cell-to-cell variability in intracellular signaling

To measure variability in intracellular signaling, we adapted a FRET assay for chemotaxis widely used for population-level measurements with fluorescent fusions to CheY and its phosphatase CheZ (*Sourjik and Berg, 2002b*). On timescales longer than the relaxation of CheY's phosphoryla-tion/dephosphorylation cycle, the FRET level reflects the phosphorylation rate of CheY by the CheA kinase, thus providing an efficient *in vivo* measurement of the network activity (Fig. 1 - Supplement 1). Instead of the conventional CFP/YFP FRET pair we used the fluorophores YFP and mRFP1 to avoid excitation with blue light, which induces considerably stronger photoxicity and also perturbs the chemotaxis system as a repellent stimulus (*Taylor and Koshland, 1975*; *Taylor et al., 1979*; *Wright et al., 2006*). A field of *E. coli* cells expressing this FRET pair were immobilized on a glass surface imaged in two fluorescence channels, and segmented offline to compute a FRET time series for each cell in the field of view (see Materials and Methods).

For wild-type cells (Fig. 1a) we found that the ensemble mean of single-cell FRET responses, $\langle \text{FRET} \rangle(t)$, agrees well with previous population-level measurements (*Sourjik and Berg, 2002b*). Upon prolonged stimulation with a saturating dose of attractant α-methylaspartate (MeAsp), $\langle \text{FRET} \rangle(t)$ rapidly fell to zero before gradually returning to the pre-stimulus level due to adaptation. Upon removal of attractant, $\langle \text{FRET} \rangle(t)$ rapidly increased to a maximum before returning to the pre-stimulus baseline. Single-cell FRET time series, $\text{FRET}_i(t)$, had qualitatively similar profiles, but the kinetics of adaptation and response amplitudes demonstrate differences from cell to cell. For each cell, $\text{FRET}_i(t)$ is limited by the slow autophosphorylation of CheA and hence is proportional to $a[\text{CheA}]_{\text{T},i}$ (provided [CheY] and [CheZ] are sufficiently high, see Materials and Methods), in which a is the activity per kinase and $[\text{CheA}]_{\text{T},i}$ the total amount of kinases part of the receptor-kinase complex. Hence from the $\text{FRET}_i(t)$ the activity per kinase a can be readily determined by normalizing each FRET timeseries by its maximum response $a = \text{FRET}_i/\text{FRET}_{i,\text{max}}$ (Figure 1b). The steady-state activity $a_{0,i}$ is then defined as the activity before the addition of attractant. The baseline activity per cell varies from cell-to-cell a_0 (quantified by the coefficient of variation, $CV = 0.22$, Fig. 1c). The network activity controls the flagellar motor rotation, and hence this is consistent with the observation that cells in isogenic population exhibit a variable steady-state tumble frequency (*Spudich and Koshland, 1976*; *Dufour et al., 2016*).

The adaptation precision is defined as its post-adaptational activity level ($\Pi = a_{adapted,i}/a_{0,i}$), hence a precision of 1 refers to perfect adaptation. The adaptation kinetics are quantified by the recovery time $\tau_{recovery}$, the time required for each cell to recover to 50% of its post-adaptational activity level ($a_{adapted,i}$). When observing the distributions of these parameters we noted that the cell-to-cell variability is high in the precision Π (Fig. 1d, CV=0.40) but the average precision (0.79) agrees well with population measurements (*Neumann et al., 2014*). The variation is also substantial in $\tau_{recovery}$

129 (Fig. 1d, CV=0.20). This falls within the range of ~20-50% from previous reports, in which single-cell

130 recovery times were estimated from motor-rotation or swimming-behavior measurements (*Berg*

131 *and Tedesco, 1975*; *Spudich and Koshland, 1976*; *Min et al., 2012*). The time required to recover

132 from a saturating amount of attractant is determined not only by the stimulus size, but also the

133 methylation rate of receptor modification sites catalyzed by CheR and the number of such sites that

134 need to be methylated. Variability in the recovery time is thus likely to reflect cell-to-cell variability in

135 the ratio between the expression level of CheR and that of the chemoreceptor species responding

136 to ligand (Tar for the experiment in Fig. 1a).

137   Thus, single-cell FRET allows efficient measurement of single-cell signaling dynamics that, on

138 average, agree well with previous population-level FRET experiments and single-cell flagellar-based

139 experiments, thereby revealing variability in a wide variety of signaling parameters.

Diversity in the ligand response is modulated during population growth

141 The chemoreceptor clusters in *E. coli* are the central processing units and are responsible for signal

142 integration and amplification. The sensory output of the cluster, the activity of the kinase CheA,

143 is activated by a mixture of chemoreceptors. Cooperative interactions within the kinase-receptor

144 complex leads to amplifications of small input stimuli and weighting different input signals. It has

145 been shown that the composition of the receptor-kinase complexes can affect both the amplification

146 as well as the weighting of different input signals (*Ames et al., 2002*; *Sourjik and Berg, 2004*; *Kalinin*

147 *et al., 2010*), but how the amplification and integration varies across a population has not been

148 characterized. To bridge the gap between collective behavior and its underlying single-cell motility

149 it is essential to determine the variability of these important signaling parameters, as well as the

150 origin of the variability. Also, current estimates of the apparent gain in the response (defined as the

151 fractional change in output divided by fractional change in input) are based on population-averaged

152 measurements which may may not reflect single-cell cooperativity levels. In population averaged

153 measurements, the largest gain is observed in adaptation-deficient (CheRB-) cells (*Sourjik and*

154 *Berg, 2004*), in which the receptor population is homogeneous with respect to their adaptational

155 modification state and hence in these cells variability in ligand sensing can be studied separately

156 from variability induced by the adaptation enzymes.

157   We probed the ligand sensitivity of CheRB- cells (TSS58) at the single-cell level by FRET dose-

158 response measurements in which step stimuli of successively larger amplitudes were applied over

159 time (Fig. 2). Considerable variability in the response to the attractant L-serine were observed

160 across the population of immobilized cells simultaneously experiencing the same stimulus, with

161 response magnitudes often ranging from virtually zero to full response (Fig. 2a). The resulting

162 dose-response data were analyzed by fitting each individual cell's FRET response by a Hill curve of

163 the form $[1 + ([L]/K)^H]^{-1}$, where the parameters $(1/K)$ and H are defined as the sensitivity and

164 steepness, respectively, of the response. The family of dose response curves constructed from

165 this ensemble of fit parameters reveals considerable variability from cell to cell in the shape of the

166 response curve (Fig. 2b).

167 What could be the cause of the diversity in ligand response in the absence of adaptation-induced

168 heterogeneity? We reasoned that expression-level variability of the five chemoreceptor species of

169 *E. coli*, which are known to form mixed clusters with cooperative interactions (*Ames et al., 2002*;

170 *Sourjik and Berg, 2004*), could endow isogenic populations with sensory diversity. In line with this

171 idea, CheRB- cells expressing only a single chemoreceptor species (Tsr) demonstrated not only

172 higher cooperativity, but also attenuated variability in the dose-response profile from cell to cell

173 (Figure 2b-c), showing that the composition of the receptor population is important not only to

174 tune the average ligand response of a population, but also in generating a wide range of sensory

175 phenotypes within an isogenic population.

176 It has been shown that expression level of chemoreceptors changes during growth of *E. coli*

177 batch cultures: concomitant with the slowing of growth upon the transition from the exponential

178 phase towards early stationary phase, the relative expression level ratio Tar/Tsr, the two most

179 abundant chemoreceptors, increases from majority Tsr (Tar/Tsr$<$ 1) to majority Tar (Tar/Tsr$>$ 1)

180 (*Salman and Libchaber, 2007*; *Kalinin et al., 2010*). To probe the consequence of such changes for

181 ligand-sensing diversity, we measured single-cell dose response curves in populations harvested

182 at different cell densities during batch growth (Figure 2d). The resulting population-averaged

183 responses show a dependence of dose-response parameters on the optical density (O.D.) of the

184 culture, shifting from highly sensitive (low K) and highly cooperative (high H) at low cell densities

185 (OD$\approx$ 0.3) to less sensitive (high K) and less cooperative (low H) at increased cell densities (OD$\approx$ 0.45,

186 and OD $\approx$ 0.6) (Fig. 2d, open triangles, and Fig. 2 - Supplement 1). This trend is also visible at the

187 level of single cells, but we found the responses to be highly variable under each condition (Fig. 2d,

188 filled points). Remarkably, both K and H varied by over an order of magnitude, far exceeding the

189 uncertainty in parameter estimates due to experimental noise (Fig. 2 - Supplement 2).

190 To further test the idea that ligand-response diversity is governed by differences in receptor

191 expression levels, we considered the pattern of covariation between the fitted sensitivity K and

192 cooperativity H in single cells (Figure 2b, blue). In contrast to cells expressing Tsr as the only

193 chemoreceptor, in which the variability in K is only 20 % (Figure 2b, orange), single cells expressing

194 a wildtype complement of chemoreceptors demonstrated strong variation in K. This variation was

195 negatively correlated with the cooperativity H (Figure 2d). Noting that this overall pattern of covari-

196 ation agrees well with dose response parameters obtained from population-level FRET experiments

197 in which the Tar/Tsr ratio was experimentally manipulated via plasmid-based expression control

198 (Figure 2d, open triangles; data from *Sourjik and Berg* (*2004*)), we proceeded to quantitatively

199 estimate the diversity in the Tar/Tsr ratio via fits of a multi-species MWC model (*Mello and Tu, 2005*;

200 *Keymer et al., 2006*) to single-cell FRET data (see Materials and Methods). The resulting distribution

201 of single-cell Tar/Tsr estimates (Figure 2e) was dominated by Tsr in cells harvested early (OD$\approx$ 0.3)

202 but the relative contribution of Tar increased in cells harvested at later stages of growth (OD≈ 0.45

203 and OD≈ 0.6). Interestingly, in addition to this increase in the mean of the Tar/Tsr distribution

204 during batch growth, which confirms previous reports that found increased Tar/Tsr ratios at the

205 population level (*Salman and Libchaber, 2007*; *Kalinin et al., 2010*), we find that the breadth of

206 the distribution also increases at later stages of growth. Thus, modulation of receptor expression

207 during growth provides a means of tuning not only response sensitivity and cooperativity, but

208 also single-cell diversity in the response of cell populations experiencing identical changes in their

209 common environment.

210 The large variability in the Tar/Tsr ratio ($CV \approx 0.5$ at O.D.=0.45) is somewhat surprising given that

211 the mean expression level of both receptors are known to be high and of order 10^3-10^4 copies per

212 cell (*Li and Hazelbauer, 2004*). At such high expression, intrinsic noise in expression levels (i.e. due

213 to the production and degradation process of proteins, expected to scale as the square root of the

214 mean) could be as low as a few percent of the mean, and gene-expression fluctuations are expected

215 to be dominated by extrinsic noise components (i.e. those affecting regulation of gene expression,

216 which do not scale with the mean). In *E. coli*, a global survey of gene expression noise established

217 an empirical lower bound to extrinsic noise at $CV \approx 0.3$ (*Taniguchi et al., 2010*), and measurements

218 within the chemotaxis system also indicate that between a subset of chemotaxis genes, the extrinsic

219 component of covariation does approach this limit (*Kollmann et al., 2005*). Interestingly, however,

220 a recent study (*Yoney and Salman, 2015*) found using single-cell flow-cytometry a high degree of

221 variability in the ratio of Tar/Tsr promotor activities ($CV \approx 0.45$ at O.D.=0.51) comparable to the

222 range of ratios extracted from our analysis of dose response data. Given that cell-to-cell variability

223 in the Tar/Tsr ratio is much greater than achievable lower bounds of gene-expression noise in

224 bacteria, it would be interesting to investigate the mechanistic sources of this variability, such as

225 operon organization, RBS strength, and promotor stochasticity (*Frankel et al., 2014*).

226 Variability in receptor expression could also explain the distribution of adaptation precision

227 we observed in wildtype cells (Figure 1d). In a previous population-level study, it has been shown

228 that adaptation precision depends strongly on the expression-level ratio between the multiple

229 chemoreceptor species, with the highest adaptation precision being achieved when the ligand-

230 binding receptor is a minority within the total receptor population (*Neumann et al., 2014*). Thus,

231 the substantial heterogeneity in adaptation precision we observed (CV = 0.40) upon a saturating

232 MeAsp stimulus is consistent with strong variability in the Tar/Tsr ratio.

CheB phosphorylation feedback attenuates cell-to-cell variability

234 While bacteria can exploit molecular noise for beneficial diversification, variability can also limit

235 reliable information transfer and degrade sensory performance. In the framework of *E. coli*'s run-

236 and-tumble navigation strategy, chemotactic response to gradients requires that cells maintain a

237 finite tumble bias, the fraction of time a bacterium spends tumbling, and avoids extreme values

238   zero and one. The latter cases would correspond to unresponsive phenotypes that fail to switch

239   between run and tumble states in response to the environmental inputs. One important mechanism

240   that ensures responsiveness to stimuli over a broad range of input levels is sensory adaptation

241   mediated by the methyltransferase/methylesterase pair CheR/CheB. These receptor-modifying

242   enzymes provide negative feedback through the dependence of their catalytic activity on the

243   receptor's signaling state: the rate of methylation (demethylation) by CheR (CheB) is a decreasing

244   (increasing) function of receptor-kinase activity (*Borczuk et al., 1986*; *Amin and Hazelbauer, 2010*).

245   This dependence of enzyme activity on the substrate conformation provides negative integral

246   feedback that ensures precise adaptation (*Barkai and Leibler, 1997*) toward the pre-stimulus steady-

247   state activity a_0.

248   Interestingly, one of the two adaptation enzymes, CheB, can be phosphorylated by CheA, the

249   kinase whose activity CheB controls through its catalytic (demethylation) activity on receptors.

250   Effectively, this adds an additional negative feedback loop to the network, but the role of this

251   phosphorylation-dependent feedback has remained elusive since it has been shown to be dispens-

252   able for precise adaptation (*Alon et al., 1999*). Through theoretical analysis, it has been conjectured

253   that this secondary feedback loop might play a role in attenuating effects of gene-expression noise

254   (*Kollmann et al., 2005*), but experimental verification has been lacking. We therefore sought to

255   investigate the influence of perturbations to this network topology on the variability of chemotactic

256   signaling activity.

257   CheB consists of two domains connected by a flexible linker (Figure 3a). A regulatory domain,

258   with structural similarity to CheY, can be phosphorylated at residue Asp[56] (*Djordevic et al., 1998*;

259   *Stewart et al., 1990*). A catalytic domain mediates binding to specific residues on chemoreceptor

260   cytoplasmic domains and removes a methyl group added by the counterbalancing activity of

261   CheR. Phosphorylation induces a conformational change and activates CheB (CheB*) (*Djordevic*

262   *et al., 1998*; *Lupas and Stock, 1989*). Several mutants of CheB lack phosphorylation feedback while

263   retaining catalytic activity. Here, we focus on two specific mutants: CheB[D56E], which bears a point

264   mutation at the phosphorylation site, and CheB$_c$, which expresses only the catalytic domain of CheB

265   (*Stewart et al., 1990*; *Alon et al., 1999*). Cells expressing these mutants have an altered network

266   topology (Figure 3b) which lacks CheB phosphorylation feedback.

267   To study the influence of network topology on cell-to-cell variability, we expressed different forms

268   of CheB (CheB[WT], CheB[D56E], CheB$_c$) from an inducible promoter in a $\Delta cheB$ strain and measured

269   the response to a saturating amount of attractant (500 μM MeAsp). The expression levels of each

270   mutant are tuned such that they approximate the wild-type steady state activity level. The response

271   variability of CheB[WT] was, as expected, very similar to cells in which CheB is expressed from its

272   native chromosomal position (compare Fig. 3 - Supplement 1a and Fig. 1a). By contrast, cells

273   expressing either of the two CheB mutants defective in phosphorylation demonstrated increased

274   cell-to-cell variability in the steady-state activity compared to cells expressing CheB[WT]. The increased

275 variability of the CheB phosphorylation-deficient mutants (CheB^{D56E} and CheB$_c$) was manifested

276 not only in a higher coefficient of variation in a_0 (1.07 and 1.10, respectively, and WT 0.7), but also a

277 qualitatively different shape of the distribution of a_0 across the population (Figure 3c). Whereas

278 the distribution demonstrated a single peak in CheB^{WT} cells with phosphorylation feedback, the

279 distribution for the phosphorylation-feedback mutants demonstrated a bimodal shape with peaks

280 close to the extreme values $a_0 = \{0, 1\}$.

281 We tested whether these strong differences in cell-to-cell variability might be the result of gene

282 expression noise, by comparing expression-level distributions of the CheB mutants. We constructed

283 fluorescent fusions of each *cheB* allele to the yellow fluorescent protein mVenus and quantified

284 the distribution of single-cell fluorescence levels under the same induction conditions as in the

285 FRET experiments (figure 3 - Supplement 1). The ratio between the measured expression-levels

286 (CheBc:WT:D56E≈0.7:1:2.5) was compatible with expectations from the hierarchy of reported *in*

287 *vitro* catalytic rates of CheB ($k_b^{D56E} < k_b^{WT} < k_b^c$) (*Anand and Stock, 2002*; *Simms et al., 1985*; *Stewart,*

288 *1993*), and expression-level variability was very similar between the three strains (CV's of 0.87, 0.90

289 and 0.82). These findings suggest that the differences in cell-to-cell variability observed in FRET

290 are not due to differences between the expression-level distributions of the three *cheB* alleles, but

291 rather to the differences they impose on the signaling network topology.

292 What feature of the signaling network could generate such broad (and even bimodal) distri-

293 butions of a_0? It has been conjectured (*Barkai and Leibler, 1997*; *Emonet and Cluzel, 2008*) and

294 demonstrated (*Shimizu et al., 2010*) that *in vivo* the enzymes CheR and CheB operate at or near

295 saturation. An important consequence of enzyme saturation in such reversible modification cycles

296 is that the steady-state activity of the substrate becomes highly sensitive to the expression level

297 ratio of the two enzymes, a phenomenon known as zero-order ultrasensitivity (*Goldbeter and*

298 *Koshland* (*1981*); see Materials and Methods). Within the chemotaxis system, saturation of both

299 CheR and CheB can thus render the receptor modification level, and in turn, the CheA activity a_0,

300 ultrasensitive to the [CheR]/[CheB] concentration ratio. If we view this ultrasensitive mapping as a

301 transfer function f between the ratio [CheR]/[CheB] and the steady-state activity a_0,

$$a_0 = f([CheR]/[CheB])$$

then its characteristic steep sigmoidal profile can impose bimodality in the methylation level, and hence also in the activity of steady-state CheA activity, a_0, even at quite modest input variances for distributions of the ratio $P_{RB}([CheR]/[CheB])$. This is because the manner in which the transfer function f filters the [CheR]/[CheB] distribution,

$$P(a_0) = \frac{P_{RB}(f^{-1}(a_0))}{\left| f'(f^{-1}(a_0)) \right|}.$$

302 spreads the narrow range in the [CheR]/[CheB] distribution $P_{RB}([CheR]/[CheB])$ over which $f([CheR]/[CheB])$

303 is steep across a broad range in a_0. Thus, even if expression-level noise for both CheR and CheB are

304 modest, an ultrasensitive transfer function f can effectively amplify the variation in [CheR]/[CheB],

305 and if the distribution of the latter ratio, P_{RB}([CheR]/[CheB]) extends below and above the narrow

306 region over which f is steep, the decreased slope of f (i.e. lower f'([CheR]/[CheB])) in those flank-

307 ing regions will tend to increase the weight on both sides of the broad $P(a_0)$ distribution to produce

308 a bimodal profile. On the other hand, if the network topology effectively reduces the steepness of f,

309 the resulting $P(a_0)$ will have a reduced variance for the same input P_{RB}([CheR]/[CheB]) (Figure 3d).

310 Could the known biochemical differences between the three forms of CheB (CheB^{WT}, CheB^{D56E},

311 CheB$_c$) explain the contrasting patterns of a_0 variability observed in our single-cell FRET experiments?

312 In the absence of any feedback, the steepness of $f(CheR/CheB)$ is solely determined by the low

313 Michaelis-Menten constants $K_{B,R}$, which corresponds to saturated kinetics of the enzymatic activity

314 of CheRB and hence ultransensitivity of the steady-state substrate activity. The expression ratio

315 of CheR/CheB which determines the crossover point (a_0=0.5) is set by the ratio of catalytic rates

316 of CheR and CheB ($k_{r,b}$). Hence the phosphorylation deficient mutants CheB^{D56E} and CheB$_c$ both

317 have steep curves but are shifted along the R/B axis due to very different catalytic rates. However,in

318 the case of phosphorylation feedback, CheB^{WT}, the same enzyme can be in two states, each

319 with equal $K_{r,b}$ but one low and one high k_r. Whether CheB is in the one state or the other is

320 determined by the activity-dependent phosphorylation feedback. As a result, the curve of CheB^{WT}

321 is activity dependent ($f(a, CheR/CheB)$) and changes with activity by shifting between the two

322 curves corresponding to the extremes of all phosphorylated or all unphosphorylated. Effectively,

323 this makes the resulting curve f less steep. The mean of the distributions P_{RB} are tuned such

324 to get the same mean activity level ($\langle a_0 \rangle$), but the same variance in P_{RB} leads to very wide $P(a_0)$

325 distributions in absence of phosphorylation, while phosphorylation feedback ensures a much

326 smaller, single-peaked distrubtion.

327 It has also been conjectured that the CheB phosphorylation feedback is responsible for the

328 highly nonlinear kinetics of recovery from repellent (or attractant removal) responses *Shimizu et al.*

329 (*2010*). Indeed, in cells expressing CheB$_c$, the kinetics of recovery from the response to removal

330 of 500 μM MeAsp after adaptation appeared qualitatively different from that in cells expressing

331 wildtype CheB, lacking the characteristic rapid recovery and instead appearing more symmetric with

332 the CheR-mediated recovery upon addition of a saturating dose of attractant (Fig. 3 - Supplement

333 3). By contrast, CheB^{D56E} was found to still possesses a fast component, despite being defective

334 in phosphorylation, albeit also with somewhat slower kinetics than wt. In summary, the clearest

335 difference between wildtype and phosphorylation-defective CheB mutants is found in the variability

336 of the steady-state signal output (i.e. kinase activity).

337 The bimodal distribution in kinase activity we observed in the phosphorylation-deficient CheB

338 mutants implies that a large fraction of cells have a CheY-P concentration far below or far above the

339 motor's response threhold and hence will impair chemotactic responses to environmental gradients.

340   Consistent with this idea, in motility-plate experiments (Supplementary Figure 3 - Supplement 4) we

341   found that chemotactic migration on soft-agar plates was severely compromised for both $CheB^{D56E}$

342   and $CheB_c$ compared to $CheB_{WT}$, indicating that the phosphorylation feedback is important for

343   efficient collective motility.

Protein-signaling noise generates large temporal fluctuations in network output

345   The slow kinetics of the adaptation enzymes CheR and CheB have been hypothesized to play a

346   role not only in determining the steady-state kinase activity a_0, but also in generating temporal

347   fluctuations of the intracellular signal (*Korobkova et al., 2004*; *Emonet and Cluzel, 2008*; *Park et al.,*

348   *2010*; *Celani and Vergassola, 2012*). We found substantial differences between wildtype (CheRB+)

349   and adaptation-deficient (CheRB-) cells in the variability of their FRET signals across time (Fig. 4).

350   The effect is clearly visible upon comparing long (~1h) FRET time series obtained from cells of these

351   two genotypes (Figure 4a). The FRET signal in wildtype cells demonstrated transient excursions

352   from the mean level that were far greater in amplitude than those in CheRB- cells. This amplitude

353    $\eta \equiv \sigma_a/\langle a \rangle$ was quantified by computing the variance of each single-cell time series, low-pass filtered

354   with a moving average filter of 10s, and shows that the fluctuation amplitudes are much larger

355   in wildtype cells compared to adaptation-deficient cells ($\langle \eta \rangle$ =0.09 and 0.44, Fig. 4b). Importantly,

356   these experiments were carried out under conditions in which no protein synthesis can occur due

357   to auxotrophic limiation (see Materials and Methods), thus ruling out gene-expression processes as

358   the source of these fluctuations.

359   Power spectral density (PSD) estimates computed from such time series confirm a nearly

360   flat noise spectrum for CheRB- cells, whereas CheRB+ cells demonstrated elevated noise at low

361   frequencies (Fig. 4c). The amplitude of these low-frequency noise components do clearly vary from

362   cell to cell, as can be gleaned in the diversity of single-cell power spectra. To quantify this protein-

363   level noise due to CheR/CheB activity, we describe the fluctuating signal as an Ornstein-Uhlenbeck

364   (O-U) process, with relaxation timescale τ and diffusion constant c, which can be interpreted as

365   a linear-noise approximation (*Van Kampen, 1981*) to the full stochastic chemical kinetics of the

366   network controlling the mean kinase activity a (*Emonet and Cluzel, 2008*):

$$\frac{da}{dt} = -\frac{1}{\tau_m}a(t) + \sqrt{c}\Gamma(t) \tag{1}$$

367   where $\Gamma(t)$ is a Gaussian white noise process. The parameters τ_m and c for each cell are readily

368   extracted via the power-spectrum solution of the O-U process:

$$S_a(\omega) = \frac{2c\tau^2}{1 + (2\pi\omega\tau_m)^2} + E \tag{2}$$

369   where we have added to the standard Lorentzian solution (*Gillespie, 1996*) a white-noise term E

370   that may vary from cell to cell to account for experimental shot noise in the photon-limited FRET

371 signal. Single-cell PSD data were well fit by Eq. 2 (Figure 4d), and the average of extracted single-cell

372 fluctuation timescales ($\langle \tau_m \rangle = 12.6s$) (Figure 4e) are in good agreement with previously reported

373 correlation times of flagellar motor switching (*Park et al., 2010*; *Korobkova et al., 2004*), as well

374 as the kinetics of CheRB-mediated changes in receptor modification from *in vivo* measurements

375 using radioactively labeled methyl groups (*Lupas and Stock, 1989*; *Terwilliger et al., 1986*). The

376 variance of the fluctuations obtained from the fits of the PSD, $\sigma_a = \sqrt{c\tau_m/2}$ yielded very similar noise

377 amplitudes $\eta_{OU} \equiv \sigma_{a,OU}/\langle a \rangle$ as calculated from the time series ($\langle \eta_{OU} \rangle = 0.42$, Fig. 4 - Supplement

378 3). We note that these noise levels are larger than expected - in a considerable fraction of cells,

379 the standard deviation of fluctuations is comparable to the mean level of activity, and the steady-

380 state fluctuations span the full range of kinase activity (see e.g. that represented by the red curve

381 in Fig. reffig:results4a). Previous studies had predicted a value of $\sim 10 - 20\%$, based either on

382 reported fluctuation amplitudes of motor switching (*Korobkova et al., 2004*; *Tu and Grinstein, 2005*)

383 or biochemical parameters of the intracellular signaling network (*Emonet and Cluzel, 2008*; *Shimizu*

384 *et al., 2010*) and is also highly variable ($\sigma_\eta = 0.24$) from cell to cell.

385 In summary, we confirmed the presence of strong temporal fluctuations in single-cell chemo-

386 taxis signaling attributable to the stochastic kinetics of the adaptation enzymes CheR/CheB, and

387 further found that the amplitude of these fluctuations vary considerably across cells in an isogenic

388 population.

Receptor-kinase fluctuations in the absence of adaptation reveal two-level switching

391 The fluctuation amplitude η in CheRB+ cells (Fig. 4b) is much greater than previous estimates from

392 pathway-based models that considered zero-order ultrasensitivity in the enzymatic activities of

393 CheR and CheB (*Emonet and Cluzel, 2008*) and receptor cooperativity (*Shimizu et al., 2010*) as

394 possible mechanisms that amplify noise originating in the stochastic kinetics of receptor methyla-

395 tion/demethylation. A plausible explanation for the latter discrepancy is that receptor cooperativity,

396 which can amplify not only ligand signals but also fluctuations in receptor methylation levels (*Duke*

397 *and Bray, 1999*; *Shimizu et al., 2003*; *Mello et al., 2004*), is actually much stronger at the single-cell

398 level than was previously estimated from population-level FRET measurements. The dose-response

399 data for CheRB- cells presented in this study (Fig. 2) clearly demonstrate that single-cell dose-

400 response curves tend to be steeper than those obtained from fits to the population average. Yet

401 another (though not exclusive) possibility is that there exist significant sources of signaling noise

402 that are independent of enzymatic receptor modification. Although we found that the noise am-

403 plitude η was much lower than wildtype in unstimulated CheRB- cells (Fig. 4), if the cooperative

404 switch-like signaling response of these cells to chemoattractant stimulation (Fig. 2) apply also to

405 other perturbations, it is possible that the strong activity bias in the absence of chemoeffectors

406 ($a_0 \approx 1$) masks noise contributions that would be observable if receptors were tuned to the more

responsive regime of intermediate activity. In wildtype cells, such a tuning is achieved by the balance between CheR and CheB activities, which sets the steady-state receptor-kinase activity to an intermediate value ($a_0 \approx 0.2$-0.5; see Fig. 1).

We reasoned that in CheRB- cells, tuning the activity to an intermediate level by adding and sustaining a sub-saturating dose of attractant could reveal additional noise sources, if present and of significant strength. To maximize detection sensitivity, we focused on cells expressing Tsr as the sole chemoreceptor in a CheRB- background, which demonstrate the highest cooperativity in ligand responses and hence could be expected to strongly amplify also noise sources relevant to signaling (Fig. 2b). To test the effect of bringing the system to the responsive regime, we applied first a large saturating dose of Tsr's cognate ligand L-serine, followed by a prolonged stimulus of a magnitude close to the dose-response parameter K, eliciting a half-maximal population-level response (Fig. 5a). During the second stimulus, which was sustained for several minutes, the population-level response remained approximately constant. Strikingly, however, the time series of single-cell responses demonstrated strong deviations from the population average (Fig. 5b). Whereas all cells responded identically to the saturating dose of attractant, the behavior during the sub-saturating step was highly diverse. Some cells (11/141) showed no apparent response in kinase activity, whereas in others (32/141) complete inhibition was observed (Fig. 5b, yellow curves). The majority cells (98/141), however, had an intermediate level of activity when averaged over time, but demonstrated strong temporal fluctuations, often with magnitudes exceeding those observed in wildtype cells.

We further noted that within this subset of cells with large temporal fluctuations, a large fraction (54/98) demonstrated fluctuations that resemble rapid step-like transitions between discrete levels of relatively stable activity that could be identified as peaks in the distribution of activity values across time (Fig. 5b, marginal histograms). Among these "stepper" cells, the majority (37/54) appeared to transition between 3 or more discrete activity levels (Fig. 5b, brown curve), whereas the remaining sizable minority of steppers (17/54) demonstrated binary switching between two discrete levels corresponding to to the maximum ($a \approx 1$) and minimum ($a \approx 0$) receptor-kinase activity states (Fig. 5b, red curve). The remaining fraction of cells (44/98) demonstrated fluctuations that were also often large but in which discrete levels could not be unambiguously assigned (Fig. 5b, black curve). The numbers of cells corresponding to each of the categories described above are summarized in Fig. 5c.

The observation of cells that demonstrate spontaneous two-level switching is particularly surprising, given the large number of molecules involved in receptor-kinase signaling. The expression level of each protein component of the chemoreceptor-CheW-CheA signaling complex in our background strain (RP437) and growth medium (TB) has been estimated (by quantitative Western Blots) to be of order 10^4 copies/cell (*Li and Hazelbauer, 2004*). Considering that the core unit of signaling has a stoichiometric composition of receptor:W:A = 12:2:2 (monomers) (*Li and Hazelbauer, 2011*), the number of core units is likely limited by the number of receptors, leading to an estimate $10^4/12 \sim 10^3$

444   core units for a typical wildtype cell. This estimate does not apply directly to the experiments of

445   Fig. 5 because receptors are expressed from a plasmid in a strain deleted for all receptors. But the

446   FRET response amplitudes of these cells were similar to those of cells with a wildtype complement

447   of receptors, and we thus expect the number of active core units per cell in the experiments of

448   Fig. 5 to be similar to or greater than that in wildtype cells.

449   We analyzed further the temporal statistics of the discrete transitions in the subset of cells

450   exhibiting two-level switching (Fig. 5d-f). We first quantified the duration of time over which such

451   transitions in activity occur by fitting segments of the activity time series over which these switches

452   occured (Fig. 5d) with a symmetrized exponential decay function (see Materials and Methods)

453   to obtain switch durations τ_+ and τ_- for upward and downward transitions, respectively. The

454   fitted values for τ_+ and τ_- correspond to the duration over which the activity trajectory traverses a

455   fraction $1 - e^{-1}$ of the transition's full extent, and were found to be similar between switches in both

456   directions: $\langle \tau_+ \rangle \pm \sigma_{\tau_+} = 4.2 \pm 2.2$ s and $\langle \tau_- \rangle \pm \sigma_{\tau_-} = 3.5 \pm 3.2$ s (Fig. 5e).

457   We then considered the duration of time between switching events. We defined $\Delta t_{up,k}$ and

458    $\Delta t_{down,k}$ as the duration of the k-th time interval between transitions with high- and low-activities,

459   respectively (Fig. 5d), and computed the average over all k of $\Delta t_{up/down,k}$ for each individual cell to

460   estimate its residence timescales $\tau_{up/down}$ for states of high/low activity, respectively. From each

461   cell's set of intervals $\{\Delta t_{up/down,k}\}$ we also computed a parameter $a_{1/2}$, defined as the fraction of

462   time the cell spent in the high activity level, as a measure of its time-averaged activity during the

463   sub-saturating (20μM) L-serine stimulus that yielded a population-averaged response $\langle a \rangle \approx 1/2$

464   (see Materials and Methods).

465   We found that the logarithms of the residence times scale approximately linearly with $\ln[a_{1/2}/(1-$

466    $a_{1/2})]$ (Fig. 5f). The latter can be considered a free-energy difference $(-\Delta G) = G_{down} - G_{up}$ between the

467   inactive and active states of an equilibrium two-state switching process in which the time-averaged

468   activity $a_{1/2}$ is given by the probability of being in the active state, $a_{1/2} = p(\text{active}) = [1 + e^{\Delta G}]^{-1}$. The

469   residence time in each state can then be described by an Arrhenius-type relation with attempt rate

470   for barrier crossing τ_r and the height of the energy barrier,

$$\tau_{down} = \tau_r \exp\left[-\gamma_{down}\Delta G / k_B T\right]$$

$$\tau_{up} = \tau_r \exp\left[-\gamma_{up}\Delta G / k_B T\right]$$

(3)

471   in which the constants γ_{down} and γ_{up} describe how the barrier heights of the down and up states

472   depend on the free-energy difference $\Delta G = \ln[(1 - a_{1/2})/a_{1/2}]$. We find $\gamma_{down} = -0.4 \pm 0.1$, $\gamma_{up} = 0.6 \pm 0.1$,

473   and the attempt timescale τ_r, defined here as equivalent to $\tau_{up} = \tau_{down}$ when $a_{1/2} = 1/2$, was found

474   to be 110 ± 10 s.

475   In summary, these data demonstrate the existence of a signaling noise source that is indepen-

476   dent of the adaptation enzymes CheR/CheB. The fluctuations they generate can be very strong in

477 cells expressing Tsr as the sole chemoreceptor, leading to two-level switching in a subset of cells.

478 The latter observation suggests that cooperativity among signaling units in chemoreceptor arrays

479 can reach extremely high values, with up to $\sim 10^3$ units switching in a cooperative fashion. The

480 temporal statistics of these two-level switches are consistent with a barrier-crossing model in which

481 the residence time of both states depend on the activity bias $a_{1/2}$.

Discussion

483 The single-cell FRET measurements described here allowed us to quantify variability in a variety

484 of signaling parameters of the bacterial chemotaxis system, both across cells in a population

485 and within individual cells over time. By imaging many (up to ~ 100) cells simultaneously, we are

486 able to collect single-cell statistics at high throughput to build up single-cell statistics. Although

487 single-cell experiments have a long history in studies of bacterial chemotaxis (*Berg and Brown,*

488 *1972*; *Spudich and Koshland, 1976*; *Block et al., 1982*; *Korobkova et al., 2004*; *Dufour et al., 2016*),

489 nearly all examples to date have relied on measurements of flagellar motor output (in either

490 tethered or swimming cells). A major advantage of the FRET approach is that it provides a direct

491 measurement of intracelluar signaling that bypasses the noisy behavior of the flagellar motor (a

492 stochastic two-state switch), thereby enabling accurate and efficient determination of signaling

493 parameters.

From gene-expression noise to network-level diversity

495 A key feature of bacterial chemotaxis as an experimental system is that one can study *in vivo*

496 signaling and behavior in a manner that is decoupled from gene expression and growth. Being an

497 entirely protein-based signaling network, chemotaxis signaling responses do not require changes in

498 gene expression, and the relatively short timescales of signaling reactions (subsecond to minutes)

499 are well separated from those of changes in protein counts due to gene expression noise (minutes

500 to hours). The ensemble of single-cell FRET time series measured in each of our experiments

501 thus provide a snapshot of cell-to-cell variability due to stochastic gene expression in a variety of

502 signaling parameters.

503 Our data revealed high variability in important signaling parameters connected to the adaptation

504 system (Fig. 1). In the case of the variability in recovery times (CV=0.20), this is likely due to variability

505 in the CheR/receptor ratio from cell to cell. What consequences might such variability have on

506 chemotactic behavior? A recent theoretical study has established that long (short) adaptation times

507 are better suited for maximizing chemotactic migration rates in shallow (steep) gradients (*Frankel*

508 *et al., 2014*). Thus, variability in adaptation times could partition the population into cells that will be

509 more efficient in running up steep gradients, while others are specialists in climbing shallow ones.

510 Interestingly, it was also found that optimal performance at each gradient involves tuning not only

511 the adaptation time, but also other parameters such as swimming speed or tumble bias, leading

512 to a selective pressure not only for the distribution of individual parameters, but also correlations
513 among them (*Frankel et al., 2014*; *Waite et al., 2016*). Whether such correlated variation exists
514 among signaling parameters would be a fruitful avenue for future single-cell FRET studies.

515   In the ligand response of the network, we observed large cell-to-cell variability in the sensitivity
516 ($1/K$) and steepness (H) of dose-response relations, for cells with a wildtype receptor population
517 (Fig. 2). Using a mixed-species MWC model (*Mello and Tu, 2005*), we were able to estimate the Tar/Tsr
518 ratio in single cells, which spans a broad range from nearly zero to more than two. This strong
519 variability in the receptor-cluster composition has the potential to dramatically impact behavior.
520 In their natural habitats, cells likely experience a variety chemoeffector gradients simultaneously,
521 each associated with an unknown fitness payoff for chemotactic pursuit. Generating diversity in the
522 chemoreceptor ratio, which has been shown to determine which gradient to climb when challenged
523 with such conflicting possibilities (*Kalinin et al., 2010*), could allow the isogenic population to hedge
524 its bets to maximize net fitness gains. The Tar/Tsr ratio has also been shown to play an important
525 role in setting the preferred temperature for thermotaxis (*Salman and Libchaber, 2007*; *Yoney and*
526 *Salman, 2015*). Variability in Tar/Tsr would allow diversification of the preferred temperature across
527 cells in the population, which will promote spreading of bacteria in environments with temperature
528 gradients. Finally, when chemotactic bacteria colonize an initially nutrient-rich environment, they
529 are known to successively exploit resources by emitting multiple traveling waves of chemotactic
530 bacteria, each of which consumes and chases by chemotaxis a different nutrient component
531 outward from the colony origin (*Adler, 1966*). Our observation that the population diversity in
532 receptor ratios, and hence chemotactic preference, varies concomitantly with population growth
533 could provide a means to tune the population fractions that engage in such excursions into virgin
534 territory, and those that remain for subsequent exploitation of remaining resources. Thus, the
535 diversity in ligand response and preference generated by variability in the Tar/Tsr ratio could have
536 nontrivial consequences in a variety of behavioral contexts encountered by isogenic chemotactic
537 (and thermotactic) populations.

538 **Suppression of gene expression noise by CheB phosphorylation feedback**

539 The role of phosphorylation feedback has been a long standing open question in the field of
540 bacterial chemotaxis signaling, ever since its presumed role in providing precise adaptation was
541 decisively ruled out by *Alon et al.* (*1999*). In the ensuing years, a diverse set of hypotheses have
542 been proposed to explain its purpose. Apart from precise adaptation, CheB phosphorylation has
543 been suggested as possibly responsible for the non-linear response of CheB activity to changes
544 in CheA kinase activity (*Shimizu et al., 2010*; *Clausznitzer et al., 2010*), ligand sensitivity of wild-
545 type cells (*Barkai et al., 2001*), and has been implicated theoretically as a possible mechanism to
546 buffer gene-expression noise to suppress detrimental variability in the steady-state kinase activity
547 (*Kollmann et al., 2005*). Here, we tested the latter hypothesis, by severing the phosphorylation

548 feedback loop as a possible noise-reduction mechanism. Our single-cell FRET data revealed that,

549 not only does CheB phosphorylation feedback strongly attenuate the magnitude of variability in

550 the steady-state kinase activity a_0, it also qualitatively changes the shape of the distribution $P(a_0)$

551 across cells to convert an otherwise bimodal distribution into a unimodal one (Fig 3d). The highly

552 polarized bimodal distribution of steady-state activities in CheB phosphorylation mutants are likely

553 detrimental, as they could drive a_0 of a large fraction of the population too far from the flagellar

554 motor's steep response threshold (*Cluzel et al., 2000*; *Yuan and Berg, 2013*) to effectively control

555 swimming. The observation of a bimodal $P(a_0)$ in the absence of phosphorylation feedback is

556 consistent with a previous modeling study by *Emonet and Cluzel* (*2008*) in that the parameters of

557 the CheR- and CheB-catalyzed covalent modification cycle appear to satisfy conditions for zero-order

558 ultrasensitivity (*Goldbeter and Koshland, 1981*), which has been hypothesized to provide a source

559 of slow and large amplitude temporal fluctuations with possible benefits for chemotaxis in certain

560 environments (see below). The fact that CheB phosphorylation seems to strongly attenuate the

561 steepness of the ultrasensitive relationship $a_0 = f([R]/[B])$ between kinase activity and the [R]/[B]

562 ratio suggests that zero-order might not suffice to explain the large amplitude temporal fluctuations

563 we observed in wildtype cells (see below).

Diversity in temporal noise: bet-hedging across exploration and exploitation strategies

566 In addition to cell-to-cell variability in signaling parameters, single-cell FRET allowed us to resolve

567 temporal fluctuations in signaling about the steady-state output within individual cells. In wild-type

568 cells, we found that the steady-state activity fluctuates slowly (Fig. 4, correlation time $\tau \approx 10s$) with

569 a large amplitude ($\eta = \sigma_a/\langle a \rangle \approx 40\%$), but this amplitude also varies significantly from cell to cell

570 ($CV \approx 0.6$). Fluctuations on this timescale were absent in CheRB- cells defective in receptor methy-

571 lation/demethylation, indicating that these fluctuations are generated by stochastic processes in

572 the activity of the adaptation enzymes CheR and CheB. Whereas the fluctuation correlation time

573 τ in our FRET experiments was in close agreement with those from previously reported flagellar

574 motor switching experiments (*Korobkova et al., 2004*; *Park et al., 2010*), the fluctuation amplitude

575 $\langle \eta \rangle \approx 40\%$ was surprisingly large. Theoretical analysis of the motor-based noise measurements (*Tu*

576 *and Grinstein, 2005*) had predicted a more modest noise level of intracellular noise, at 10-20% of

577 the mean. The discrepancy is likely due, at least in part, to the recently discovered adaptation at

578 the level of the flagellar motor (*Yuan et al., 2012*), which must effectively act as a highpass filter

579 that attenuates frequencies near or below a cutoff frequency determined by its own characteristic

580 timescale for adaptation. The fluctuation amplitude η was also much greater than previous esti-

581 mates from pathway-based models. A possible explanation is the amplification of noise by receptor

582 cluster cooperativiy, which our results show to be much higher compared to previous estimates

583 based on population-averaged measurements. Another possibility is an additional source of noise.

584 In cells with a pure cluster composition we clearly demonstrate this possibility. Investigating how 585 both noise sources contribute in the case of mixed receptor clusters (e.g. CheRB- cells) and the 586 amplification magnitude (dose response curves in CheRB+ cells) should be an interesting direction 587 for future study.

588   The temporal noise we observed could have profound implications for *E. coli*'s random-walk 589 motility strategy, because slow fluctuations in the intracellular signal can enhance the likelihood of 590 long run events and stretch the tail of the run-length distribution to yield power-law-like switching-591 time distributions over a range of time scales (*Korobkova et al., 2004*; *Tu and Grinstein, 2005*). 592 Such non-exponential statistics are known to yield superior foraging performance in environments 593 where resource distribution is sparse (*Viswanathan et al., 1999*), and temporal fluctuations in 594 run-tumble behavior has also been shown theoretically to enhance climbing of shallow gradients 595 by generating runs that are long enough to integrate over the faint gradient a detectable difference 596 in ligand input (*Flores et al., 2012*; *Sneddon and Emonet, 2012*). Hence, the noise generated by the 597 adaptation system can be advantageous in resource-poor environments (*deserts*) in which efficient 598 exploration of space for sparsely distributed sources (*oases*) is of utmost importance. By contrast, 599 strong temporal noise clearly degrades response fidelity in rich environments where the gradient 600 signal is strong enough for detection with short runs, and might also complicate coordination of 601 cells in collective behaviors such as the aforementioned traveling-wave exploitation of nutrients. 602 Our finding that the noise amplitude varies strongly from cell to cell thus suggests that isogenic 603 populations might be hedging their bets by partitioning themselves between specialists for local 604 exploitation of identified resource patches and those for long-range exploration in search for new 605 ones.

Giant fluctuations and digital switching in adaptation deficient cells

607 We found the most dramatic temporal fluctuations in adaptation-deficient (CheRB-) cells expressing 608 Tsr as the sole chemoreceptor species (Fig. 5). When brought close to their dose-response transition 609 point (K) by attractant stimulation, these cells demonstrated strong temporal fluctuations, revealing 610 that there exist sources of signal fluctuations that are independent of CheR and CheB activity. 611 The origin of these adaptation-independent fluctuations remain unknown, but in broad terms, 612 one can envisage that they are due to either intrinsic sources (i.e. fluctuations arising within 613 the components of the receptor-kinase complex), extrinsic sources (i.e. fluctuations in other 614 cellular processes / environmental variables), or both. Possible to intrinsic sources include coupled 615 fluctuations in protein conformations (*Duke and Bray, 1999*; *Shimizu et al., 2003*; *Mello et al., 2004*; 616 *Skoge et al., 2011*), the slow-timescale changes in receptor "packing" that have been observed by 617 fluorescence anisotropy measurements(*Frank and Vaknin, 2013*; *Vaknin, 2014*), and the stochastic 618 assembly dynamics of receptor clusters (*Greenfield et al., 2009*). Possible extrinsic sources include 619 fluctuations in metabolism, membrane potential, or active transport/consumption of ligand. Many

620 of these possibilities could be tested by experiments of the type presented here with appropriate

621 mutant strains and environmental controls, and present promising directions for future research.

622 The adaptation-independent fluctuations we observed were not only large in amplitude but

623 often (though not always) took the form of discrete steps in activity, in some cases between

624 only two levels. Two-state descriptions of receptor signaling are a common feature of nearly all

625 mechanistic models of bacterial chemotaxis signaling addressing both cooperativity (*Duke and*

626 *Bray, 1999*; *Shimizu et al., 2003*; *Mello et al., 2004*; *Mello and Tu, 2005*; *Keymer et al., 2006*) and

627 adaptation (*Asakura and Honda, 1984*; *Barkai and Leibler, 1997*; *Morton Firth et al., 1999*; *Endres*

628 *and Wingreen, 2006*; *Tu et al., 2008*), yet direct evidence for two-state switching by receptor-kinase

629 complexes has been lacking. Although as noted above, it is yet possible that the two-level switching

630 we observed (Fig. 5a,b) is due to extrinsic noise sources (e.g. metabolism or transport), the temporal

631 statistics we observed (Fig. 5d-f) are compatible with a simple model in which two stable signaling

632 states are separated by an energy barrier sensitive to both environmental stimuli and internal cell

633 variables.

634 Regarding cells that exhibited step-like transitions among more than two stable states, a plausi-

635 ble interpretation is that the underlying transitions are actually two-level, but the receptor-kinase

636 population is partitioned into two or more disjoint signaling arrays, and that the observed FRET

637 signals represent the sum of the stochastic two-level activities of these independently switching

638 arrays. For cells in which there is sufficient spatial separation between chemoreceptor clusters, it

639 could be possible to test this hypothesis by conducting on the same set of cells both FRET measure-

640 ments and receptor-cluster imaging to relate the number of distinct step sizes to the number of

641 observed clusters.

642 If the stochastic two-level switching we observed is indeed due to intrinsic sources of noise, it

643 would strongly suggest (as discussed in Results) that at least many hundreds, if not thousands of

644 receptor-kinase units are switching in a cooperative fashion. The rather long timescale associated

645 with intervals between switches ($\approx 10^2$ s) is indicative of their large size, and is also clearly distinct

646 from the methylation-dependent fluctuation timescale (≈ 10 s) observed in CheRB+ cells. The

647 switching duration (≈ 4 s) , is also much slower than the sub-second response to attractant stimuli

648 (*Segall et al., 1982*; *Sourjik and Berg, 2002a*). Interestingly, these timescales ($\sim 10^2$ s and $\sim 10^0$ s for

649 inter-switch intervals and switch durations, respectively) are approximately 10^2-fold longer than

650 those measured by *Bai et al.* (*2010*) for the two-state switching of the flagellar motor ($\sim 10^0$ s and

651 $\sim 10^{-2}$ s for inter-switch intervals and switch durations, respectively), whose C-ring is composed of

652 $\sim 10^1$ allosteric units, approximately 10^2-fold less than the $\sim 10^3$ units we estimate for the number

653 of receptor-kinase units per cell in our experiments. The study of *Bai et al.* (*2010*) demonstrated

654 impressive agreement between those temporal statistics and predictions of a "conformational

655 spread" model (*Duke et al., 2001*; *Bray and Duke, 2004*), an adaptation of the equilibrium Ising

656 model for ferromagnetism (*Ising, 1925*). It would be interesting to investigate whether similar

657 Ising-type models for the receptor lattice (*Duke and Bray, 1999*; *Shimizu et al., 2003*; *Mello et al.,*

658 *2004*; *Skoge et al., 2006*) can explain the timescales observed in our receptor-kinase switching data.

659 Although our results indicate that, at least to a first approximation, receptor-kinase switching

660 can be treated as a thermally driven barrier-crossing process, we note that our data do not rule out

661 the possibility of non-equilibrium switching mechanisms (*Tu, 2008*). Indeed, despite the success of

662 equilibrium models in closely matching a wealth of data on the flagellar motor switch (*Bai et al.,*

663 *2010*), recent experiments have revealed new evidence that switching of the motor C-ring likely

664 includes also an active component, effectively utilizing part of the energy dissipated in motor torque

665 generation to enhance sensitivity (*Wang et al., 2017*). Like the motor C-ring switch, whose state is

666 only observable when coupled to rotation driven by dissipative proton conduction, essentially all

667 experimental methods available to study receptor-kinase signaling involve coupling to a dissipative

668 process (ATP hydrolysis by CheA) for readout. The experimental access to receptor-kinase temporal

669 statistics afforded by single-cell FRET holds promise to help discriminate possible equilibrium and

670 non-equilibrium mechanisms for signal processing within this remarkable protein circuit.

Concluding remarks

672 We described a new single-cell FRET technique capable of resolving intracellular signaling dynamics

673 in live bacteria over extended times. Our results highlight how a protein-based signaling network

674 can either generate or attenuate variability, by amplifying or filtering molecular noise of different

675 molecular origins. Gene expression noise is harnessed, on the one hand, to generate diversity in

676 the ligand response of isogenic populations, or attenuated, on the other the hand, in the control

677 of steady-state signal output. In addition, we showed that signaling noise generated at the level

678 of interacting gene products can have a profound impact. Stochastic protein-protein interactions

679 within the signaling network, as well as other "extrinsic" fluctuations, can be amplified by the

680 signaling network to generate strong temporal temporal fluctuations in the network activity.

Materials and Methods

Strains and Plasmids

All strains used are descendants of *E. coli* K-12 HCB33 (RP437). Growth conditions were kept uniform by transforming all strains with two plasmids. All strains and plasmids are shown in Tables 1 and 2.

The FRET acceptor-donor pair (CheY-mRFP and CheZ-YFP) is expressed in tandem from a IPTG inducible pTrc99A plasmid, pSJAB12 or pSJAB106, with respective induction levels of 100 and 50 μM IPTG. The differences between pSJAB12 and pSJAB106 are i) the presence of a noncoding spacer in pSJAB106 to modify the ribosome binding site of CheZ *Salis et al.* (*2009*), such that CheZ is expressed approximately 3 fold less, and ii) a A206K mutation in YFP to enforce monomerity. We also used pVS52 (CheZ-YFP) and pVS149 (CheY-mRFP1) to express the fusions from separate plasmids with induction levels of 50 uM IPTG and 0.01 % arabinose, respectively. We transformed the FRET plasmids in adaptation-proficient strain (VS104) to yield CheRB+ and adaptation- (VS149) to get CheRB-. For attachment with sticky flagella from pZR1 we used the equivalent strains in *fliC* background (VS115 and TSS58).

Experiments with Tsr as the sole chemoreceptor were performed in UU2567 or TSS1964, in which the native FliC gene is changed to sticky FliC (FliC*). Tsr is expressed from pPA114 Tsr, a pKG116 derivative, at with an induction of 0.6 μM NaSal.

For the experiments with the CheB mutants, pSJAB12 was transformed into VS124 together with plasmids expressing CheB^{WT}, CheB^{D56E} and truncated mutant CheB$_c$ (plasmids pVS91, pVS97 and pVS112, respectively, with induction levels of 1.5E-4, 6E-4 and 3E-4 % arabinose.

Abbreviation	Strain	Source	Relevant Genotype	plasmid 1	plasmid 2
WT / CheRB+	VS115	V. Sourjik	ΔYZ ΔFliC	pSJAB106	pZR1
WT / CheRB+	VS104	*Sourjik and Berg* (*2002b*)	ΔCheYZ	pVS52	pVS149
WT / CheRB+	VS104		ΔCheYZ	pSJAB12	pBAD33
WT / CheRB+	VS104		ΔCheYZ	pSJAB106	pBAD33
CheRB-	TSS58	*this work*	ΔRBYZ ΔFliC	pSJAB106	pZR1
CheRB-	VS149	*Sourjik and Berg* (*2004*)	ΔRBYZ	pVS52	pVS149
CheRB-	VS149		ΔCheRBYZ	pSJAB12	pBAD33
CheRB-	VS149		ΔCheRBYZ	pSJAB106	pBAD33
CheBc	VS124	*Clausznitzer et al.* (*2010*)	ΔCheBYZ	pSJAB12	pVS112
D56E	VS124		ΔCheBYZ	pSJAB12	pVS97
WT CheB	VS124		ΔCheBYZ	pSJAB12	pVS91
Tsr only	UU2567	*Kitanovic et al.* (*2015*)	ΔCheRBYZ,ΔMCP^a	pSJAB106	pPA114 Tsr
Tsr only	TSS1964	*this work*	ΔCheRBYZ,ΔMCP FliC*	pSJAB106	pPA114 Tsr
ΔCheB	UU2614	J.S. Parkinson	CheB Δ(4-345)	pTrc99a	pVS91,97,11

All strains are descendants of E. coli K-12 HCB33 (RP437). In all FRET experiments, strains carry two plasmids and have resistance for chloramphenicol and ampicillin.

Table 1. Strains used in this study.

^{a}all five chemoreceptor genes *tar tsr tap trg aer* deleted

Name	Product	System	Ind	Res	Source
pVS52	CheZ-5G-YFP	pBAD33	ara	cam	*Sourjik and Berg* (*2002b*)
pVS149	CheY-5G-mRFP1	pTrc99a	IPTG	amp	*Sourjik and Berg* (*2002b*)
pSJAB12	CheZ-5G-YFP / CheY-5G-mRFP1	PTrc99a	IPTG	amp	This work
pSJAB106	CheZ-5G-YFP [a] / CheY-5G-mRFP1	PTrc99a	IPTG	amp	This work
pVS91	CheB [b]	pTrc99a	ara	cam	*Liberman et al.* (*2004*)
pVS97	CheB-D56E [c]	pBAD33	ara	cam	*Clausznitzer et al.* (*2010*)
pVS112	CheBc [d]	pBAD33	ara	cam	V. Sourjik
pSJAB 122	CheBc-GS4G-mVenus	pBAD33	ara	cam	This work
pSJAB 123	CheB(D56E)-GS4G-mVenus	pBAD33	ara	cam	This work
pSJAB 124	CheB-GS4G-mVenus	pBAD33	ara	cam	This work
pZR 1	FliC* [e]	pKG116	NaSal	cam	This work
pPA114 Tsr	Tsr	pPA114	NaSal	cam	*Ames et al.* (*2002*)

Table 2. Plasmids used in this study.

[a] Contains a A206K mutation to enforce monomerity.
[b] expresses WT CheB
[c] carries a point mutation D56E in CheB
[d] expresses only residues 147-349 of CheB, preceded by a start codon (Met)
[e] expresses sticky FliC element *Scharf et al.* (*1998*)

FRET Microscopy

Föster Resonance Energy Transfer [FRET] microscopy was performed as previously reported (*Sourjijk et al., 2007*; *Vaknin and Berg, 2004*). Cells were grown to OD=0.45-0.5 in Tryptone Broth (TB) medium from a saturated overnight culture in TB, both with 100 μg/mL ampicillin and 34 μg/mL chloramphenicol and appropriate inducers in the day culture. For the FRET experiments we used Motility Media (MotM) (*Shimizu et al., 2006*), in which cells do not grow and protein expression is absent. Cells were washed in 50 mL MotM, and then stored 0.5-6 h before experiment. In the dose-response curve experiments and the temporal fluctuation measurements, cells were stored up to three hours at room temperature to allow for further red fluorescence maturation. A biological replicate or independent FRET experiment was defined as a measurement from separately grown cultures, each grown on a separate day.

Cells were attached by expressing sticky FliC elements from a pKG116 plasmid, induced with 2μM Sodium Salicylate (NaSal), or with Poly-L-Lysine (Sigma), or with anti-FliC antibodies column purified (Using Protein A sepharose beads, Amersham Biosciences) from rabbit blood serum and pre-absorbed to FliC- cells (HCB137, gifts from Howard Berg). We found FRET experiments with sticky FliC to have the highest signal-to-noise ratio.

Fluorescent images of the cells were obtained with a magnification of 40-100x (Nikon instruments). For excitation of YFP, we either used 514 nm laser excitation set to 30 mW for 2 ms or an LED system (CoolLED, UK) with an approximate exposure time of 40 ms to approximate the same illumination intensity per frame. The sample was illuminated stroboscopically with a frequency

721 between 1 and 0.2 Hz. RPF excitation was performed by 2ms exposure of 60 mW 568 nm laser or

722 equivalent with LED to measure acceptor levels independently from FRET.

723   Excitation light was sent through a 519 nm dichroic mirror (Semrock, USA). Epifluorescent

724 emission was led into an Optosplit (Cairn Research, UK) with a second dichroic mirror 580 nm and

725 two emission filters (527/42 nm and 641/75 nm, Semrock, USA) to project the RFP and YFP emission

726 side by side on an EM-CCD (Princeton Instruments, USA) with multiplication gain 100. All devices

727 were controlled through custom-written software.

Image processing

729 Images were loaded and analyzed by means of in-house written scripts in MATLAB and Python.

730 Images were corrected for inhomogeneous illumination. Single cells were selected by image

731 segmentation on the donor emission with appropriate filter steps to remove clusters of cells or

732 cells improperly attached to the coverslip. At the position of each cell a rectangular ROI is defined in

733 which all fluorescence intensity is integrated. For experiments in which the concentration of donor

734 molecules may influence the FRET signal, the experiments on the CheB mutants, segmentation

735 was done separately for each frame to determine the cell shape and then linking these segmented

736 images with a tracking algorithm (*Crocker and Grien, 1996*), afterwards, fluorescence intensities

737 are normalized for the cell size (mask surface area) in segmentation and cells with low acceptor

738 intensities were excluded from the analysis. The ROI for the donor intensity were subsequently used

739 to obtain the acceptor intensity per cell, both in photon-count per pixel. Fluorescence intensities

740 were corrected for bleaching by fitting a linear, single exponential or double exponential function to

741 the fluorescence decay, separately for both donor and acceptor. Cells in which the intensity decay

742 cannot accurately be corrected were excluded from the analysis.

FRET analysis

744 The FRET signal is calculated from fluorescent time series. We observe changes in the ratio $R = A/D$,

745 in which A and D are the fluorescence intensities of the acceptor and donor. In previous population-

746 averaged FRET experiments the FRET per donor molecule ($\Delta D/D_0$) is calculated as (*Sourjik and*

747 *Berg, 2002b*; *Sourjijk et al., 2007*):

$$\frac{\Delta D}{D_0} = \frac{\Delta R}{\alpha + R_0 + \Delta R} \tag{4}$$

748 in which R_0 is the ratio in absence of FRET, $\alpha = |\Delta A/\Delta D|$ is a constant that depends on the

749 experimental system (in our case $\alpha = 0.30$) and the change in ratio as a result of energy transfer

750 ΔR. ΔR and R_0 are obtained through observing the ratio just after adding and removing saturated

751 attractant stimuli. This expression is convenient for population FRET since is invariant to attachment

752 densities of a population. However, in single-cell FRET this expression may generate additional

753 variability in FRET due to variable donor levels from cell to cell. Hence it is more convenient to

754 define the FRET levels in terms of the absolute change in donor level ΔD, since this reflects the

755   number of resonance energy transfer pairs

$$\text{FRET}(t) = \Delta D = D_0 \frac{\Delta R}{\alpha + R_0 + \Delta R} \tag{5}$$

756   Since FRET occurs only when CheY-P and CheZ interact, the FRET level is proportional to the

757   concentration of complex [Yp-Z]. If we assume the CheY-P dephosphorylation by CheZ follows

758   Michaelis-Menten kinetics we can describe the [Yp-Z] concentration in terms of the activity of the

759   kinase CheA. For this, we assume the system is in steady-state for timescales much larger than

760   CheY phosphorylation-dephosphorylation cycle ($\approx 100\,\text{ms}$). In that case, the destruction rate should

761   equal the rate of CheA phosphorylation and hence the FRET signal is proportional to the activity

762   per kinase a and the amount of CheA in the kinase-receptor complex (*Sourjik and Berg, 2002b*;

763   *Oleksiuk et al., 2011*):

$$\text{FRET} \propto [\text{Yp-Z}] = a\frac{k_A}{k_Z}[\text{CheA}] \approx a\frac{k_A}{k_Z}[\text{CheA}]_\text{T} \tag{6}$$

764   This last step is only valid if we further assume CheA autophosphorylation being the rate-limiting

765   step. This is the case only if sufficient amounts of CheZ and CheY present in the cell. We have

766   found that the FRET level initially increases with donor (CheZ) levels, but then saturates and remains

767   constant for CheY and CheZ (see Fig. 3 - Supplement 2).

768   In many cases the most relevant parameter is the normalized FRET response. The FRET level

769   reaches maximum if all kinases are active ($a \approx 1$). In case of CheRB+ cells, this is the case when

770   removing a saturating amount of attractant after adaptation (*Sourjik and Berg, 2002b*). For CheRB-

771   cells the baseline activity is (*Sourjik and Berg, 2002b*; *Shimizu et al., 2010*) close to 1. Hence

772   the normalized FRET $\text{FRET}(t)/\text{FRET}_\text{max}$ represents the activity per kinase $a(t)$ and is the relevant

773   parameter for many quantitative models for chemoreceptor activity (*Tu, 2013*).

$$a(t) = \frac{\text{FRET(t)}}{\text{FRET}_{max}} \tag{7}$$

774   and from $a(t)$ the steady-state activity a_0 can be determined by averaging $a(t)$ over baseline values

775   before adding attractant stimuli.

Power Spectral Density Estimates

777   From FRET time series of length T and acquisition frequency f we calculated Power Spectral Density

778   [PSD] estimates as

$$S_{\text{FRET}}(\omega) = \frac{1}{T}|\mathscr{F}(\omega)|^2 \tag{8}$$

779   in which $\mathscr{F}(\omega)$ is the discrete-time Fourier transform. We only consider positive frequencies and

780   multiply by two to conserve power.

781   To study the influence of experimental noise and the effect of estimating τ and c from a finite

782   time window, we generated O-U time series using the update formula (*Gillespie, 1996*)

$$X(t + \Delta t) = X(t) - \tau^{-1}\Delta t + c^{1/2}n(\Delta(t))^{1/2} \tag{9}$$

783   in which n denotes a sample value from a normal variable. To the generated time series Gaussian

784   white noise was added to simulate experimental noise. The experimental noise amplitude was

785   obtained from the average power at high frequencies.

Two-state switching analysis

787   We obtained switching durations by fitting the function

$$a(t) = \frac{1}{2} \pm \frac{1}{2}\frac{t - t_0}{|t - t_0|}(1 - e^{-2|t-t0|/\tau_\pm}) \tag{10}$$

788   to the normalized FRET time series in a 30-second time window, approximately ±15 s from t_0. The

789   residence times $\Delta t_{up,i,k}$ and $\Delta t_{down,i,k}$ of event k in cell i were defined by the time between transitions

790   or the beginning/end of the 20 μM stimulus time window. The steady-state activity during activity

791   was then calculated as

$$a_{1/2,i} = \frac{\sum_k \Delta t_{up,i,k}}{\sum_k \Delta t_{up,k} + \sum_k \Delta t_{up,i,k}} \tag{11}$$

792   and for the residence times we take the mean over k to get τ_{down} and τ_{up}. If we treat the system as

793   an equilibrium process we can use the Arrhenius equations that describe the residence times as a

794   function of the distance to the energy barrier

$$\tau_{down} = \tau_r \exp\left[\gamma_{down}\ln\left[a_{1/2}/(1 - a_{1/2})\right]/k_BT\right]$$
$$\tau_{up} = \tau_r \exp\left[\gamma_{up}\ln\left[a_{1/2}/(1 - a_{1/2})\right]/k_BT\right] \tag{12}$$

795   in which γ_{down} and γ_{up} are constants corresponding to the slopes of $\ln\tau_{down}$ and $\ln\tau_{up}$ against

796   $\ln\left[a_{1/2}/(1 - a_{1/2})\right]$, respectively. The fit parameters and standard error are obtained with the robustfit

797   function in Matlab (statistics toolbox).

Dose Response Curve Analysis

799   Normalized FRET responses to different levels of ligand are fit to a hill curve of the form

$$a = \frac{[L]^H}{[L]^H + [K]^H} \tag{13}$$

This can be connected to an MWC-type model (*Monod et al., 1965*) of receptor cluster activity

(*Shimizu et al., 2010*) in the regime $K_I << [L] << K_A$, resulting in the correspondence key

$$H = N$$

$$K = K_I e^{f_m(m)}$$

800 which relates the Hill slope directly to the cluster size N, and sensitivity K to the methylation energy

801 of the receptor. We plot K on a logarithmic scale to scale linearly with energy.

802 To obtain expression level estimates of different receptor species we use a different MWC model.

803 Following **Mello and Tu** (*2005*), we use as an expression for the normalized response of cells to

804 ligand $[L]$ serine

$$a = \frac{\epsilon_0 \epsilon_S^{N_S} \epsilon_A^{N_A} (1 + C[L]/\tilde{K})^{N_s}}{(1 + [L]/\tilde{K})^{N_s} + \epsilon_0 \epsilon_S^{N_S} \epsilon_A^{N_A} (1 + C[L]/\tilde{K})^{N_s}} \tag{14}$$

805 in which N_A is the number of Tar receptors in the cluster and N_S is the number of Tsr receptors.

806 Parameters ϵ_A, ϵ_S, ϵ_0 are the energies corresponding to binding of ligand to Tar, Tsr and the other

807 three receptors and are the same for each cell, like C and $\tilde{K}$ which describe the disassociation

808 constant for the active state as $K_A = \tilde{K}/C$, while N_A and N_T may vary from cell to cell. This yields

809 the minimization problem for all 128 cells

$$\min \sum_i^{N_{cells}} \sum_j^{N_{stim}} (m_{i,j} - a_{i,j})^2 \tag{15}$$

810 in which $m_{i,j}$ the measured FRET response normalized to the response amplitude of cell i to stimulus

811 L_j. This function was minimized using the matlab function fmincon (optimization toolbox). The

812 total number $N_T = N_A + N_S$ is limited to 32. When fitting the model used the energy parameters ϵ

813 from reference **Mello and Tu** (*2005*) where used as initial guess with a maximum of $\pm 5\%$ deviation.

814 This yielded an estimate of N_A and N_S for each cell. Under the assumption that receptor clusters

815 are well-mixed, this yields a Tar/Tsr ratio of N_A/N_S.

Parameter	Start Value *Mello and Tu* (*2007*)	Final Value
C	0.314	0.29
ϵ_0	0.80	0.84
ϵ_A	1.23	1.29
ϵ_S	1.54	1.61
$\tilde{K}$	–	21.2 μM

Table 3. List of global parameters used for model of Mello and Tu. In these fits, $\tilde{K}$ is a free parameter while others are constrained $\pm 5\%$ by published values.

816 **Ultrasensitive adaptation model of phoshorylation feedback**

We model the methylation-demethylation cycle of the receptors as a Goldbeter-Koshland cycle

(**Goldbeter and Koshland, 1981**; **Emonet and Cluzel, 2008**). For simplicity, we do not explicitly

describe the methylation and demethylation of the receptors explicitly but instead assume that

CheR (R) activates the receptor-kinase complex directly (A*), and that CheB (B) deactivates it (A).

$$A + R \rightarrow A^* + R$$

$$A^* + B \rightarrow A + B$$
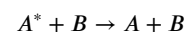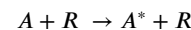
817 We now assume that these reactions follow Michaelis-Menten kinetics and the total amount of

818 kinase complexes is constant ($A_T = A^* + A$). Hence the change in $\mathscr{A} = A^*/A_T$ can be described as

$$\frac{d\mathscr{A}}{dt} = v_r \frac{1 - \mathscr{A}}{K_r + 1 - \mathscr{A}} - v_b \frac{\mathscr{A}}{\mathscr{A} + K_b} \tag{16}$$

819 in which v_r and v_b are the rates for the reactions mediated by R and B, respectively. The Michaelis-

820 Menten constants K_b and K_r are in units of A_T and are therefore dimensionless numbers. We are

821 interested in the steady-state level $\mathscr{A}_0$ and its dependence on the kinetic parameters in equation 16.

822 This is described by the Goldbeter-Koshland function **Tyson et al.** (**2003**), an exact solution to the

823 system in case [R] and [B] are much smaller than $[A]_T$.

$$\mathscr{A}_0[v_r, v_b, K_r, K_b] = \frac{2 v_r K_r}{(v_b - v_r + v_b K_b + v_r K_r + \sqrt{(v_b - v_r + v_b K_b + v_r K_r)^2 - 4(v_b - v_r)v_r K_r}} \tag{17}$$

824 The shape of this curve is sigmodal if the Michaelis-Menten constants K_r and K_b are much smaller

825 than one. For CheB phosphorylation, we assume the phosphorylation rate depends linearly on

826 active CheA and write

$$\frac{d[\text{Bp}]}{dt} = k_p [\text{B}] \mathscr{A}(v_r, v_b, K_b, K_r) - k_{dp}[\text{Bp}] \tag{18}$$

827 with the corresponding conservation law $B_T = B_P + B$. For the case for wild-type CheB, with phosphory-

828 lation feedback, the rates can be described in terms of catalytic rate times the enzyme (subspecies)

829 concentration

$$v_b = k_b([\text{B}_T] - [\text{Bp}]) + M k_b [\text{Bp}]$$

$$v_r = k_r [\text{R}] \tag{19}$$

in which M stands for the ratio of demethylation rates of unphosphorylated and phosphorylated

CheB. The fraction of the phosphorylated CheB, $[\text{Bp}]/[\text{B}]_T$, which is given by $k_{dp}/(k_p + k_{dp})$ then

determines the effective activity of CheB. Equation 18 is solved numerically using Mathematica for

[Bp] and the result is substituted in equation 17. In the absence of feedback, the activity can be

directly calculated from equation 17 with the rates being simply

$$v_b = k_b [\text{B}]$$

$$v_r = k_r [\text{R}]$$

830 We only need to consider the ratio of rate constants k_r and k_b which determines at which expression

831 ratio [CheR]/[CheB] the activity equals 1/2. We assume $k_r = k_b$ for simplicity, since the shape of the

832 curve from Eq. 17 is not affected, it only shifts the the curve along the horizontal axis. Similarly, we

833 only consider the ratio of phosphorylation and dephosphorylation rates. This leaves the system of

834 equations above only has a few parameters: $K_{b,r}$; M; and the ratios k_r/b_b and k_p/k_{dp}, M. In table 4,

835 the parameters used for the calculations are listed.

836 We first fixed the phosphorylation rates $k_p > 2k_{dp}$. This means that the steady-state phospho-

837 rylated level of CheB $[B_p]/[B_T]$ at activity $\approx 1/3$ is around 15 %. This parameter is not constrained

838 by any direct observation, but it is clear the system benefits from a relatively low fraction of

839 phosphorylation, to be able to up and down regulate the levels effectively upon changes in activity.

840   Generally, we assume D56E to behave like unphosphorylated CheB. The gain in catalytic rate of

841 activated CheB is estimated to be nearly a 100 fold, but this does not agree with the expression

842 level differences between the different CheB mutants so we made a conservative estimate of 15

843 (the attenuating effect increases with the gain). CheBc behaves approximately like phosphorylated

844 CheB (albeit with increase of only 7 compared to D56E), qualitatively consistent with measured

845 *in vitro* rates for CheBc and phosphorylated intact CheB *Anand and Stock* (*2002*). The difference

846 between predicted rates and might be due to the fact that the rate experiments were performed

847 *in vitro*. Michaelis Menten constants used in the model are lower than 1, but how low is not well

848 constrained by data, and estimations do not take into account the possible attenuating effect of

849 phosphorylation. Our experimental data on the distribution of a_0 implies the sigmodial curve is

850 steep in the absence of phosphorylation and hence that K_b and K_r are quite small. The variability in

851 a_0 for CheBc is lower than D56E, implying that the curve is less steep and hence we have chosen

852 are K_r which is not quite as low as D56E.

853   To simulate gene expression noise, we simulated [CheR]/[CheB] log-normal distributions with $\sigma =$

854 0.18 for all three strains. The mean of the distribution was chosen to yield an average steady-state

855 network activity (a_0) of 0.4. The resulting distribution of a_0 was calculated using the corresponding

Goldbeter-Koshland function for each genotype.

Parameter	Value	Literature	Source
k_r/k_p	1	0.75	*Shimizu et al.* (*2010*)
k_{dp}/k_p	2	$k_p = 0.37^{-1}$	*Kentner and Sourjik* (*2009*)
K_r	0.03	«1	*Emonet and Cluzel* (*2008*)
K_b	0.03	«1	*Emonet and Cluzel* (*2008*)
$K_b(CheBc)$	0.2	«1	
M (WT)	15	100	*Anand and Stock* (*2002*)
M (CheBc)	7	15	*Simms et al.* (*1985*)

Table 4. List of parameters used for Goldbeter-Koshland description of CheB phosphorylation feedback.

856

References

Adler J. Chemotaxis in bacteria. Science. 1966 Aug; 153(3737):708–716. http://dx.doi.org/10.1126/science.153.3737.708, doi: 10.1126/science.153.3737.708.

Alon U, Surette MG, Barkai N, Leibler S. Robustness in bacterial chemotaxis. Nature. 1999 Jan; 397(6715):168–171. http://dx.doi.org/10.1038/16483, doi: 10.1038/16483.

Ames P, Studdert CA, Reiser RH, Parkinson JS. Collaborative signaling by mixed chemoreceptor teams in Escherichia Coli. PNAS. 2002; 99:7060–65. doi: 10.1073/pnas.092071899.

Amin D, Hazelbauer G. Chemoreceptors in signalling complexes: shifted conformation and asymmetric coupling. Mol Microbiol. 2010 Dec; 78:1313–23. doi: 10.1111/j.1365-2958.2010.07408.x.

Anand GS, Stock AM. Kinetic Basis for the Stimulatory Effect of Phosphorylation on the Methylesterase Activity of CheB. Biochemistry. 2002; 41:6752–6760.

Asakura S, Honda H. Two-state model for bacterial chemoreceptor proteins. The role of multiple methylation. J Mol Biol. 1984; 176:349–69.

Bai F, Branch R, Nicolau D, Pilizota T, Steel B, Maini P, Berry R. Conformational spread as a mechanism for cooperativity in the bacterial flagellar switch. Science. 2010; 327:685–9. doi: 10.1126/science.1182105.

Barkai N, Alon U, Leibler S. Robust amplification in adaptive signal transduction networks. C R Acad Sci Paris, Série IV. 2001; p. 871–877.

Barkai N, Leibler S. Robustness in simple biochemical networks. Nature. 1997 Jun; 387(6636):913–917. http://dx.doi.org/10.1038/43199, doi: 10.1038/43199.

Berg HC, Brown DA. Chemotaxis in Escherichia coli analysed by Three-dimensional Tracking. Nature. 1972 Oct; 239(5374):500–504. http://dx.doi.org/10.1038/239500a0, doi: 10.1038/239500a0.

Berg HC, Tedesco PM. Transient Response to Chemotactic Stimuli in Escherichia coli. PNAS. 1975 Aug; 72(8):3235–3239. http://dx.doi.org/10.1073/pnas.72.8.3235, doi: 10.1073/pnas.72.8.3235.

Block S, Segall J, Berg H. Impulse responses in bacterial chemotaxis. Cell. 1982; 31:215–26.

Borczuk A, Staub A, Stock J. Demethylation of bacterial chemoreceptors is inhibited by attractant stimuli in the complete absence of the regulatory domain of the demethylating enzyme. Biochem Biophys Res Commun. 1986 Dec; 141:918–23.

Bray D, Duke T. Conformational spread: The Propagation of Allosteric States in Large Multiprotein Complexes. nnu Rev Biophys Biomol Struct. 2004; 33:53–73. doi: doi: 10.1146/annurev.biophys.33.110502.132703.

Bray D, Levin MD, Morton-Firth CJ. Receptor clustering as a cellular mechanism to control sensitivity. Nature. 1998 05; 393(6680):85–88. http://dx.doi.org/10.1038/30018.

Celani A, Vergassola M. Nonlinearity, Fluctuations, and Response in Sensory Systems. Physical Review Letters. 2012 Jun; 108:258102+. http://dx.doi.org/10.1103/physrevlett.108.258102, doi: 10.1103/physrevlett.108.258102.

Clausznitzer D, Oleksiuk O, Løvdok L, Sourjik V, Endres RG. Chemotactic Response and Adaptation Dynamics in Escherichia Coli. PLoS Computational Biology. 2010 May; 6(5):e1000784+. http://dx.doi.org/10.1371/journal.pcbi.1000784, doi: 10.1371/journal.pcbi.1000784.

894 **Cluzel P**, Surette M, Leibler S. An Ultrasensitive Bacterial Motor Revealed by Monitoring Signaling Proteins in
895   Single Cells. Science. 2000 Mar; 287(5458):1652–1655. http://dx.doi.org/10.1126/science.287.5458.1652, doi:
896   10.1126/science.287.5458.1652.

897 **Crocker**, Grien. Methods of Digital Video Microscopy for Colloidal Studies. Journal of colloid and interface
898   science. 1996; (179):298–310.

899 **Djordevic S**, Goudreau PN, Xu Q, Stock AM, West AH. Structural basis for methylesterase CheB regulation by a
900   phosphorylation-activated domain. PNAS. 1998 February; 95:1381–1386.

901 **Dufour Y**, Gillet S, Frankel N, Weibel D, Emonet T. Direct Correlation between Motile Behavior and Protein
902   Abundance in Single Cells. PLoS Comput Biol. 2016; 12. doi: 10.1371/journal.pcbi.1005041.

903 **Duke T**, Le Novère N, D B. Conformational spread in a ring of proteins: a stochastic approach to allostery. J Mol
904   Biol. 2001; 308:541–53.

905 **Duke T**, Bray D. Heightened sensitivity of a lattice of membrane receptors. PNAS. 1999; 96:10104–8. doi:
906   10.1073/pnas.96.18.10104.

907 **Eldar A**, Elowitz MB. Functional roles for noise in genetic circuits. Nature. 2010 Sep; 467(7312):167–173.
908   http://dx.doi.org/10.1038/nature09326, doi: 10.1038/nature09326.

909 **Elowitz MB**, Levine AJ, Siggia ED, Swain PS. Stochastic Gene Expression in a Single Cell. Science. 2002 Aug;
910   297(5584):1183–1186. http://dx.doi.org/10.1126/science.1070919, doi: 10.1126/science.1070919.

911 **Emonet T**, Cluzel P. Relationship between cellular response and behavioral variability in bacterial
912   chemotaxis. PNAS. 2008 Mar; 105(9):3304–3309. http://dx.doi.org/10.1073/pnas.0705463105, doi:
913   10.1073/pnas.0705463105.

914 **Endres R**, Wingreen N. Precise adaptation in bacterial chemotaxis through "assistance neighborhoods". PNAS.
915   2006; 103:13040–13044. doi: 10.1073/pnas.0603101103.

916 **Flores M**, Shimizu TS, ten Wolde PR, Tostevin F. Signaling Noise Enhances Chemotactic Drift of *E. coli*. Physical
917   Review Letters. 2012 Oct; 109:148101+. http://dx.doi.org/10.1103/physrevlett.109.148101, doi: 10.1103/phys-
918   revlett.109.148101.

919 **Frank V**, Vaknin A. Prolonged stimuli alter the bacterial chemosensory clusters. Mol Microbiol. 2013; 88:634–44.
920   doi: 10.1111/mmi.12215.

921 **Frankel NW**, Pontius W, Dufour YS, Long J, Hernandez-Nunez L, Emonet T, Marder E. Adaptability of non-genetic
922   diversity in bacterial chemotaxis. eLife. 2014 Oct; p. e03526+. http://dx.doi.org/10.7554/elife.03526, doi:
923   10.7554/elife.03526.

924 **Gillespie DT**. The mathematics of Brownian motion and Johnson noise. American Journal of Physics. 1996
925   March; 64:225–240.

926 **Goldbeter A**, Koshland DE. An amplified sensitivity arising from covalent modification in biological systems.
927   PNAS. 1981 Nov; 78(11):6840–6844. http://dx.doi.org/10.1073/pnas.78.11.6840, doi: 10.1073/pnas.78.11.6840.

928 **Greenfield D**, McEvoy AL, Shroff H, Crooks GE, Wingreen NS, Betzig E, Liphardt J. Self-Organization of the
929   Escherichia coli Chemotaxis Network Imaged with Super-Resolution Light Microscopy. PLoS Biology. 2009; 7.
930   doi: https://doi.org/10.1371/journal.pbio.1000137.

931 **Ising E**. Beitrag zur Theorie des Ferromagnetismus. Z Physik. 1925; 31:253. doi: 10.1007/BF02980577.

932 **Kalinin Y**, Neumann S, S V, Wu M. Responses of Escherichia coli bacteria to two opposing chemoattractant
933 gradients depend on the chemoreceptor ratio. Journal of Bacteriology. 2010; 192(7):1796–1800.

934 **Kentner D**, Sourjik V. Dynamic map of protein interactions in the Escherichia Coli chemotaxis pathway. Molecular
935 Systems Biology. 2009; .

936 **Keymer JE**, Endres RG, Skoge M, Meir Y, Wingreen NS. Chemosensing in Escherichia coli: Two regimes of
937 two-state receptors. Proceedings of the National Academy of Sciences. 2006 Feb; 103(6):1786–1791. http:
938 //dx.doi.org/10.1073/pnas.0507438103, doi: 10.1073/pnas.0507438103.

939 **Kitanovic S**, Ames P, Parkinson JS. A Trigger Residue for Transmembrane Signaling in the Escherichia coli Serine
940 Chemoreceptor. J Bacteriology. 2015 Aug; 197:2568–79. doi: 10.1128/JB.00274-15.

941 **Kollmann M**, Løvdok L, Bartholomé K, Timmer J, Sourjik V. Design principles of a bacterial signalling network.
942 Nature. 2005 Nov; 438(7067):504–507. http://dx.doi.org/10.1038/nature04228, doi: 10.1038/nature04228.

943 **Korobkova E**, Emonet T, Vilar JM, Shimizu TS, Cluzel P. From molecular noise to behavioural variability in a single
944 bacterium. Nature. 2004 Apr; 428(6982):574–578. doi: 10.1038/nature02404.

945 **Lazova MD**, Ahmed T, Bellomo D, Stocker R, Shimizu TS. Response Rescaling in Bacterial Chemotaxis. PNAS.
946 2011; 108(33):13870–75.

947 **Lazova MD**, Butler MT, Shimizu TS, Harshey RM. Salmonella chemoreceptors McpB and McpC mediate a
948 repellent response to L-cystine: a potential mechanism to avoid oxidative conditions. Molecular Microbiology.
949 2012 May; 4(84):697–711.

950 **Li GW**, Burkhardt D, Gross C, Weissman JS. Quantifying absolute protein synthesis rates reveals principles
951 underlying allocation of cellular resources. Cell. 2014 apr; 157(3):624–35. http://www.ncbi.nlm.nih.gov/
952 pubmed/24766808, doi: 10.1016/j.cell.2014.02.033.

953 **Li M**, Hazelbauer GL. Cellular stoichiometry of the components of the chemotaxis signaling complex. Journal
954 of bacteriology. 2004 Jun; 186(12):3687–3694. http://dx.doi.org/10.1128/jb.186.12.3687-3694.2004, doi:
955 10.1128/jb.186.12.3687-3694.2004.

956 **Li M**, Hazelbauer GL. Core unit of chemotaxis signaling complexes. PNAS. 2011; 108:9390–5. doi:
957 10.1073/pnas.1104824108.

958 **Liberman L**, Berg HC, Sourjik V. Effect of Chemoreceptor Modification on Assembly and Activity of the Receptor-
959 Kinase Complex in *Escherichia Coli*. J of Bacteriology. 2004 Aug; 186(19):6643–46. doi: 10.1038/262467a0.

960 **Lupas A**, Stock J. Phosphorylation of N-terminal Regulatory Domain Activates the CheB Methylesterase in
961 Bacterial Chemotaxis. J of Biological Chemistry. 1989 October; 264:17337–17342.

962 **Masson JB**, Voisinne G, Wong-Ng J, Celani A, Vergassola M. Noninvasive inference of the molecular chemotactic
963 response using bacterial trajectories. PNAS. 2012 Jan; 109:1802–7. doi: 10.1073/pnas.1116772109.

964 **Mello B**, Shaw LB, Tu Y. Effects of Receptor Interaction in Bacterial Chemotaxis. Biophysical Journal. 2004 Oct;
965 87:1578–95.

Mello BA, Tu Y. An allosteric model for heterogeneous receptor complexes: Understanding bacterial chemotaxis responses to multiple stimuli. PNAS. 2005 Nov; 102(48):17354–17359. http://dx.doi.org/10.1073/pnas.0506961102, doi: 10.1073/pnas.0506961102.

Mello BA, Tu Y. Effects of adaptation in maintaining high sensitivity over a wide range of backgrounds for Escherichia Coli chemotaxis. Biophysical journal. 2007 Apr; 92(7):2329–2337. doi: 10.1529/biophysj.106.097808.

Mesibov R, Ordal GW, Adler J. The Range of Attractant Concentrations for Bacterial Chemotaxis and the Threshold and Size of Response over This Range. The Journal of General Physiology. 1973; 62(2):203–223. http://jgp.rupress.org/content/62/2/203, doi: 10.1085/jgp.62.2.203.

Min TL, Mears PJ, Golding I, Chemla YR. Chemotactic adaptation kinetics of individual Escherichia Coli cells. PNAS. 2012 june; .

Monod J, Wyman J, Changeux JP. ON THE NATURE OF ALLOSTERIC TRANSITIONS: A PLAUSIBLE MODEL. Journal of molecular biology. 1965 May; 12:88–118. http://view.ncbi.nlm.nih.gov/pubmed/14343300.

Morton Firth C, Shimizu T, Bray D. A free-energy-based stochastic simulation of the Tar receptor complex. J Mol Biol. 1999; 286:1059–74. doi: 10.1006/jmbi.1999.2535.

Neumann S, Vladimirov N, Krembel AK, Wingreen NS, Sourjik V. Imprecision of adaptation in Escherichia Coli chemotaxis. PLoS ONE. 2014; 9(1):1–6.

Oleksiuk O, Jakovljevic V, Vladimirov N, Carvalho R, Paster E, Ryu WS, Meir Y, Wingreen NS, Kollmann M, Sourjik V. Thermal Robustness of Signaling in Bacterial Chemotaxis. Cell. 2011 Apr; 145(2):312–321.

Ozbudak EM, Thattai M, Kurtser I, Grossman AD, Van Oudenaarden A. Regulation of noise in the expression of a single gene. Nature genetics. 2002 May; 31(1):69–73. doi: 10.1038/ng869.

Park H, Pontius W, Guet CC, Marko JF, Emonet T, Cluzel P. Interdependence of behavioural variability and response to small stimuli in bacteria. Nature. 2010 Dec; 468(7325):819–823. http://dx.doi.org/10.1038/nature09551, doi: 10.1038/nature09551.

Parkinson JS, Hazelbauer GL, Falke JJ. Signaling and sensory adaptation in Escherichia Coli chemoreceptors: 2015 update. Trends in Microbiology. 2015; 23(5):257–266. http://dx.doi.org/10.1016/j.tim.2015.03.003.

Raj, Van Oudenaarden A. Nature, nurture, or chance: stochastic gene expression and its consequences. Cell. 2008 oct; 135(2):216–26. http://www.pubmedcentral.nih.gov/articlerender.fcgi?artid=3118044{&}tool=pmcentrez{&}rendertype=abstract, doi: 10.1016/j.cell.2008.09.050.

Rao C, Wolf DM, Arkin AP. Control, exploitation and tolerance of intracellular noise. Nature. 2002 11; 420(6912):231–237. http://dx.doi.org/10.1038/nature01258.

Raser JM, O'Shea EK. Control of Stochasticity in Eukaryotic Gene Expression. Science. 2004; 304:1811–14. doi: 10.1126/science.1098641.

Salis HM, Mirsky EA, Voigt CA. Automated design of synthetic ribosome binding sites to control protein expression. Nature Biotechnology. 2009; .

Salman H, Libchaber A. A concentration-dependent switch in the bacterial response to temperature. Nature Cell Biology. 2007; 9(9):1098–1100. doi: 10.1038/ncb1632.

Scharf BE, Fahrner KA, Turner L, Berg HC. Control of direction of flagellar rotation in bacterial chemotaxis. PNAS. 1998; 95:201–206.

Segall JE, Block SM, Berg HC. Temporal Comparisons in Bacterial Chemotaxis. PNAS. 1986; p. 8987–8991.

Segall J, Manson M, Berg H. Signal processing times in bacterial chemotaxis. Nature. 1982; 296:855–7.

Shimizu TS, Aksenov SV, Bray D. A spatially extended stochastic model of the bacterial chemotaxis signalling pathway. Journal of molecular biology. 2003 May; 329(2):291–309. http://view.ncbi.nlm.nih.gov/pubmed/12758077.

Shimizu TS, Tu Y, Berg HC. A modular gradient-sensing network for chemotaxis in Escherichia coli revealed by responses to time-varying stimuli. Molecular Systems Biology. 2010 Jun; 6. http://dx.doi.org/10.1038/msb.2010.37, doi: 10.1038/msb.2010.37.

Shimizu TS, Delalez N, Pichler K, Berg HC. Monitoring bacterial chemotaxis by using bioluminescence resonance energy transfer: absence of feedback from the flagellar motors. PNAS. 2006; .

Simms SA, Keane MG, Stock J. Multiple forms of the CheB methylesterase in Bacterial Chemosensing. J of Biological Chemistry. 1985 August; 260:10161–10168.

Skoge M, Meir Y, Wingreen N. Dynamics of Cooperativity in Chemical Sensing among Cell-Surface Receptors. Phys Rev Lett. 2011; 107:178101. doi: https://doi.org/10.1103/PhysRevLett.107.178101.

Skoge ML, Endres RG, Wingreen NS. Receptor-Receptor Coupling in Bacterial Chemotaxis: Evidence for Strongly Coupled Clusters. Biophys J. 2006 Jun; 90(12):4317–4326. http://dx.doi.org/10.1529/biophysj.105.079905, doi: 10.1529/biophysj.105.079905.

Sneddon MW, Emonet T. Modeling cellular signaling: taking space into the computation. Nat Meth. 2012 Mar; 9(3):239–242. doi: 10.1038/nmeth.1900.

Sourjijk V, Vaknin A, Shimizu TS, Berg HC. In vivo measurement by FRET of pathway activity in bacterial chemotaxis. Methods Enzymology. 2007; (423):365–91.

Sourjik V, Berg HC. Binding of the Escherichia coli response regulator CheY to its target measured in vivo by fluorescence resonance energy transfer. PNAS. 2002 Oct; 99(20):12669–12674. http://dx.doi.org/10.1073/pnas.192463199, doi: 10.1073/pnas.192463199.

Sourjik V, Berg HC. Receptor sensitivity in bacterial chemotaxis. PNAS. 2002 Jan; 99(1):123–127. http://dx.doi.org/10.1073/pnas.011589998, doi: 10.1073/pnas.011589998.

Sourjik V, Berg HC. Functional interactions between receptors in bacterial chemotaxis. Nature. 2004 Mar; 428(6981):437–441. http://dx.doi.org/10.1038/nature02406, doi: 10.1038/nature02406.

Spudich JL, Koshland DE. Non-genetic individuality: chance in the single cell. Nature. 1976 Aug; 262(5568):467–471. http://dx.doi.org/10.1038/262467a0, doi: 10.1038/262467a0.

Stewart RC. Activating and inhibitory mutations in the regulatory domain of CheB, the methylesterase in bacterial chemotaxis. J of Biological Chemistry. 1993 January; 268:1921–1930.

Stewart RC, Roth AF, Dahlquist FW. Mutations that affect control of the methylesterase activity of CheB, a component of the chemotaxis adaptation system in E. Coli. J of Bacteriology. 1990 June; 172:3388–3399.

Taniguchi Y, Choi PJ, Li GW, Chen H, Babu M, Hearn J, Emili A, Xie XS. Quantifying E. Coli Proteome and Transcriptome with Single-Molecule Sensitivity in Single Cells. Science. 2010; 329(5991):533–539. http://www.pubmedcentral.nih.gov/articlerender.fcgi?artid=2922915{&}tool=pmcentrez{&}rendertype=abstract.

Taylor BL, Koshland DE. Electron taxis and blue light effect on bacterial chemotaxis. Journal of Bacteriology. 1975; 123:557–569.

Taylor BL, Miller JB, Warrick HM, Koshland DE. Electron acceptor taxis and blue light effect on bacterial chemotaxis. Journal of Bacteriology. 1979; 140:567–573.

Terwilliger T, Wang J, Koshland D. Kinetics of Receptor Modification. Journal of Biol Chemistry. 1986; 261:10814–20.

Tu Y. The nonequilibrium mechanism for ultrasensitivity in a biological switch: Sensing by Maxwell's demons. PNAS. 2008; 105:11737–41. doi: 10.1073/pnas.0804641105.

Tu Y. Quantitative Modeling of Bacterial Chemotaxis: Signal Amplification and Accurate Adaptation. Annual Review of Biophysics. 2013 February; 42:337–359.

Tu Y, Shimizu TS, Berg HC. Modeling the chemotactic response of Escherichia coli to time-varying stimuli. PNAS. 2008 Sep; 105(39):14855–14860. http://dx.doi.org/10.1073/pnas.0807569105, doi: 10.1073/pnas.0807569105.

Tu Y, Grinstein G. How White Noise Generates Power-Law Switching in Bacterial Flagellar Motors. Phys Rev Lett. 2005 May; 94:208101. http://link.aps.org/doi/10.1103/PhysRevLett.94.208101, doi: 10.1103/PhysRevLett.94.208101.

Tyson JJ, Chen KC, Novak B. Sniffers, buzzers, toggles and blinkers: dynamics of regulatory and signaling pathways in the cell. Current Opinion in Cell Biology. 2003 Apr; 15(2):221–231. http://view.ncbi.nlm.nih.gov/pubmed/12648679.

Vaknin A. The dynamics in the bacterial chemosensory arrays. AIP Conference Proceedings. 2014; 1610:34–40.

Vaknin A, Berg HC. Single Cell FRET imaging of phosphatase activity in the Escherichia coli chemotaxis system. PNAS. 2004 Dec; 101(49):170272–7.

Van Kampen NG. Stochastic Processes in Physics and Chemistry. Elsevier Science; 1981. http://www.amazon.com/exec/obidos/redirect?tag=citeulike07-20&path=ASIN/0444866507.

Viswanathan G, Buldyrev S, Havlin S, da Luz MGE, Raposo E, Stanley HE. Optimizing the success of random searches. Nature. 1999; 401:911–914. doi: 10.1038/44831.

Wadhams GH, Armitage JP. Making sense of it all: bacterial chemotaxis. Nature Reviews Molecular Cell Biology. 2004 Dec; 5(12):1024–1037. doi: 10.1038/nrm1524.

Waite AJ, Frankel NW, Dufour YS, Johnston JF, Long J, Emonet T. Non-genetic diversity modulates population performance. Molecular Systems Biology. 2016; 12.

Wang F, Shi H, He R, Wang R, Zhang R, Yuan J. Non-equilibrium effect in the allosteric regulation of the bacterial flagellar switch. Nature Physics. 2017; doi: 10.1038/nphys4081.

Wright S, Walia B, Parkinson JS, Khan S. Differential activation of Escherichia coli chemoreceptors by blue-light stimuli. Journal of bacteriology. 2006 Jun; 188(11):3962–3971.

1074 **Yang Y**, Pollard AM, Höfler C, Gernot Poschet G, Wirtz R M andHell, Sourjik V. Relation between chemotaxis and
1075   consumption of Amino Acids in bacteria. Molecular Microbiology. 2015; 96:1272–1282.

1076 **Yoney A**, Salman H. Precision and Variability in Bacterial Temperature Sensing. Biophysical Journal. 2015;
1077   108(May).

1078 **Yuan J**, Berg H. Ultrasensitivity of an adaptive bacterial motor. J Mol Biol. 2013 May; 425:1760–4. doi:
1079   10.1016/j.jmb.2013.02.016.

1080 **Yuan J**, Branch RW, Hosu BG, Berg HC. Adaptation at the output of the chemotaxis signalling pathway. Nature.
1081   2012 Apr; 484(7393):233–236. http://dx.doi.org/10.1038/nature10964, doi: 10.1038/nature10964.

Acknowledgments

Competing interests

The authors declare they have no financial or non-financial competing interests.

Main Figures
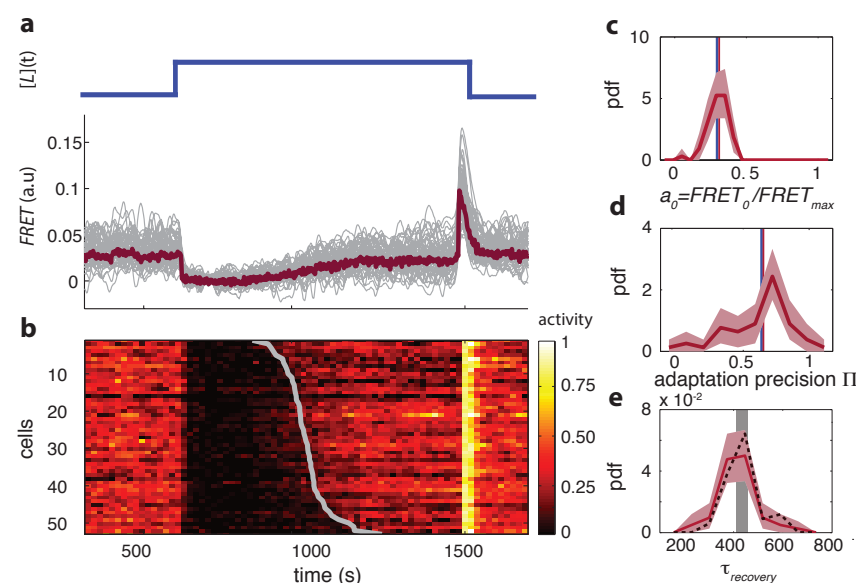
Figure 1. Single-cell FRET over extended times reveals cell-to-cell variability in signaling response. **(a)** Step-response experiment on wildtype cells (CheRB+; VS115). (Top) The ligand time series $[L](t)$ indicates the applied temporal protocol for addition and removal of 500 μM MeAsp. (Bottom) FRET response of 54 cells (grey) with the ensemble-averaged time series (dark red) overlaid from a representative single experiment. Single-cell time series were lowpass filtered with a 14s moving-average filter. **(b)** Heatmap representation of the normalized FRET response time series, with each row representing a single cell, and successive columns representing the 10s time bins in which the color-indicated activity was computed from the FRET time series. Activity was computed by normalizing FRET to the total response amplitude (Max-Min for each time series). Rows are sorted by the corresponding cell's recovery time (grey curve), defined as the time at which the activity recovered to 50 % of the activity level after adaptation (see panel e). Single-cell FRET assay schematic and image processing pipeline are shown in Figure 1 - Supplement 1. **(c)** Steady-state activity a_0 of the cells shown in panels (a-b). Also shown are the mean steady-state activity (red vertical line) and the steady-state activity of the population averaged time series (blue vertical line). **(d)** Adaptation precision Π obtained from the FRET data. An adaptation precision of 1 denotes perfect adaptation. Also shown are the mean precision (red vertical line) and the precision of the population averaged time series (blue vertical line). The mean and std of the distribution is 0.79 ± 0.32. All colored shaded areas refer to 95 % confidence intervals obtained through bootstrapping. **(e)** Recovery time of cells defined as recovery to 50% of the post-adaptational activity level (red, 54 cells) or 50% of pre-stimulus activity (black dashed, 44 cells with precision >0.5) and simulated effect of experimental noise for a population with identical recovery times (grey). The latter was obtained from a simulated data set in which 55 time series were generated as described in Figure 1 - Supplement 2. The width of the bar is defined by the mean plus (minus) the std of the simulated distribution. The mean and std of the distributions for the experimental and simulated data sets are respectively 416 ± 83 and 420 ± 35.

Figure 1 - Supplement 1 Single-cell FRET assay schematic and workflow.

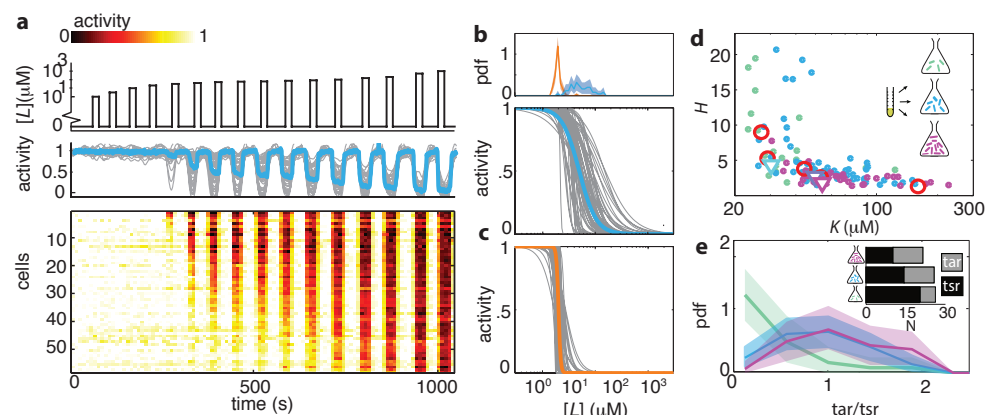**Figure 1 - Supplement 2** Influence of experimental noise on estimating recovery times.

Figure 2. Ligand dose-response parameters vary strongly across cells in an isogenic population, even in the absence of adaptation, and depend on receptor-complex composition. **(a)** Single-cell dose-response experiment on adaptation deficient (CheRB-; TSS58) cells with a wildtype complement of receptors. (Top) Temporal protocol of stimulation $[L](t)$ by the attractant L-serine. (Middle) The ensemble-averaged FRET response of the population (blue) and single cells (gray) in signaling activity of 59 cells from a single experiment, normalized to the full-scale FRET response amplitude. (Bottom) Heatmap representation of the single-cell FRET timeseries, with the rows sorted by the sensitivity K of the corresponding cell obtained from Hill-curve fits. **(b)** Family of dose response curves (gray) obtained from the Hill-curve fits to single-cell dose-response data. CheRB- cells with a wildtype complement of receptors (TSS58). The blue curve was obtained from fitting a hill function to the population-averaged time series shown in panel (a), yielding fit values K=50 μM and H=2.7. The fitted single-cell K values are shown in the histogram on top (blue). **(c)** CheRB- cells expressing only the serine receptor Tsr (UU2567). The orange curve was obtained from fits to the population average, yielding K=20 μM and H=22. The fitted single-cell K values are shown in the histogram in panel (b) (orange). **(d)** Cells from a single overnight culture were innoculated into three flasks harvested at different times during batch-culture growth growth to sample the state of the population at three points along the growth curve: at OD_{600}=0.31 (green), 0.45 (blue) and 0.59 (purple). The fits to the population-averaged time series are shown in Figure 2 - Supplement 1. Shown are Hill-curve sensitivity $(1/K)$ and cooperativity H obtained from fits to the single-cell time series, at different OD's (filled dots) together with the fit values from the population-average (triangles). Also shown are population-FRET results in which Tar and Tsr levels were controlled artificially (red circles,(*Sourjik and Berg, 2004*)). Shown are 25 out of 28 cells harvested at OD=0.31, 59 out of 64 cells at OD=0.45, 34 out of 40 cells at OD=0.59. The excluded cells had fits with a mean squared error higher then 0.05. The influence of experimental noise on the fit parameters is shown in Figure 2 - Supplement 2. **e)** Histograms of Tar/Tsr ratio obtained from fit of multi-species MWC model from reference *Mello and Tu* (*2005*) to single-cell FRET time series. The mean Tar/Tsr ratios (low to high OD) are 0.4, 0.9, and 1.2 with coefficients of variance of respectively 1.1, 0.5, and 0.4. Inset: average cluster size of Tar (grey) and Tsr (black) at different harvesting OD's obtained from the fit results in panel d.

Figure 2 - Supplement 1 Dose response curves from population averaged time series at different harvesting OD's.

Figure 2 - Supplement 2 Influence of experimental noise on fit parameters K and H.
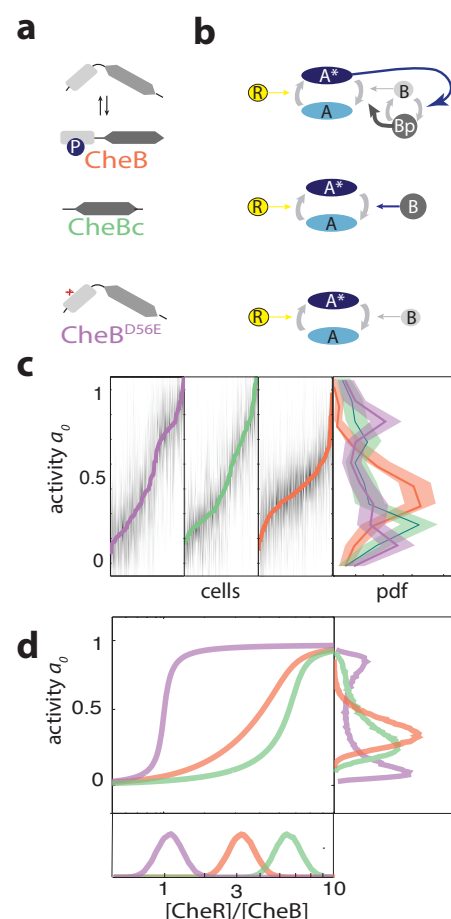
Figure 3. CheB phosphorylation feedback attenuates variability in steady-state kinase activity. **(a)** Schematic depiction of CheB activation by phosphorylation. (Top) CheB consists of two domains connected by a flexible linker. The aspartate at residue 56 can be phosphorylated. (Middle) CheBc lacks the receiver domain with the phosphorylation site. (Bottom) CheB-D56E carries a point mutation at the phosphorylation site. **(b)** Effective network topology of cells expressing WT CheB (top), CheBc (middle) and CheB-D56E (bottom). All network topologies can have perfect adaptation. Using population FRET, we found that phosphorylation feedback is not required for fast removal adaptation kinetics (Figure 3 - Supplement 3). **(c)** Heatmap representation of histograms of activity a(t) around steady-state of single-cells, from experiments as shown in Figure 3 - Supplement 1. Each colum represents a single cell, for each CheB mutant in a *cheB* background (VS124, colors as in panel (a)). The single cells are ordered by the steady-state activity a_0, which is superimposed. (right) Histograms with a_0 for each CheB mutant. All histograms contain the results for cells with a signal-to-noise ratio higher than 1 from at least 3 independent FRET experiments, which corresponds to 322 out of 373 cells (WT), 225 out of 279 cells (CheBc) and 226 out of 359 cells (D56E). Shaded regions represent bootstrapped 95% confidence intervals. We verified that the bistability was caused by clipping of extreme values due to potential FRET pair saturation, by working in a regime where the response amplitude cannot be saturated by the FRET pair (Figure 3 - Supplement 2). Furthermore, we established that the defect in phosphorylation leads to impared chemotaxis in soft agar plates (Figure 3 - Supplement 4). **(d)** A simple kinetic model of the chemotaxis network illustrates the crucial role of CheB phosphorylation feedback in circumventing detrimental bimodality in a_0. Due to saturated enzyme kinetics in the adaptation system, the transfer function between [CheR]/[CheB] expression ratio and steady-state network output a_0 can be highly nonlinear (main panel). The shape of this transfer function determines the distribution of a_0 (right panel) by transforming the distribution of [CheR]/[CheB] expression ratios (bottom panel). Shown are a CheB version with lower activity as WT (purple) and higher than WT (green), both without feedback, and one CheB species with phosphorylation feedback (orange).

Figure 3 - Supplement 3 Phosphorylation feedback is not a necessary condition for fast removal adaptation dynamics.
Figure 3 - Supplement 1 Example FRET time series and CheB localization.
Figure 3 - Supplement 2 Relation between maximum FRET response and FRET fluorophore expression levels.
Figure 3 - Supplement 4 Phosphorylation defective mutants show impaired chemotaxis on soft agar.
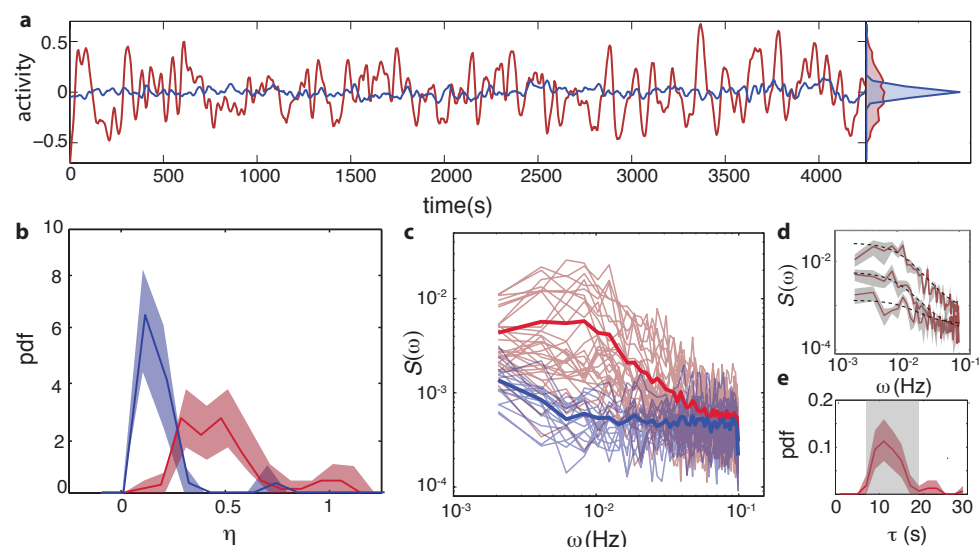
Figure 4. Temporal signal fluctuations in the absence of ligand stimulation are generated by stochastic activity of the adaptation enzymes CheR/CheB. **(a)** Representative single-cell FRET time series of steady-state fluctuations in the presence (CheRB+, VS115, red) and absence (RB-,TSS58,blue) of adaptation kinetics in normalized activity units. **(b)** Histogram of fluctuation amplitude η for both CheRB+ (89 cells, red, from 3 independent experiments) and CheRB- (33 cells, blue, from two independent experiments), extracted from calculating the standard deviation of a low-pass filtered FRET time series over a 10s window divided by the mean FRET level of a single cell. The shaded areas represents the 95% confidence interval obtained from bootstrapping. **(c)** Power spectral density (PSD) computed from single-cell FRET time series of 31 CheRB+ cells (red, from single experiment) and 17 CheRB- cells (blue, from single experiment), each from a single experiment. Thin curves in the lighter shade of each color represent Single-cell spectra, and the thick curves in the darker shade are the average of all single-cell spectra for each genotype. Note that if the PSD is calculated from the population average the effect of fluctuations are lost Figure 4 - Supplement 1. **(d)** Representative single-cell PSDs and fits by an Ornstein-Uhlenbeck (O-U) process. Shown are O-U fits (Lorentzian with constant noise floor; dashed curves) to three single-cell PSDs (solid curves). The shaded area represents the standard error of the mean for PSDs computed from nine non-overlapping segments of each single-cell time series. Fits to all cells from the same experiment are shown in (Figure 4 - Supplement 2). From the OU fit parameters the noise amplitude can be calculated (Figure 4 - Supplement 3). **(e)** Histogram of fluctuation timescales τ extracted from single-cell PSD fits (red, 75 out of 89 cells). Cells without a clear noise plateau were excluded from the analysis (Figure 4 - Supplement 3). The shaded areas represents the 95% confidence interval obtained from bootstrapping. The grey shaded area refers to the variability (mean±std) that can be explained by experimental noise and a finite time window, obtained through simulated O-U time series (see Materials and Methods).

Figure 4 - Supplement 1 PSD estimates from population-averaged time series.
Figure 4 - Supplement 2 Fits of OU process to PSD estimates from single-cell FRET time series from a representative single experiment.
Figure 4 - Supplement 3 Comparison between noise amplitudes obtained from time series and power spectra.
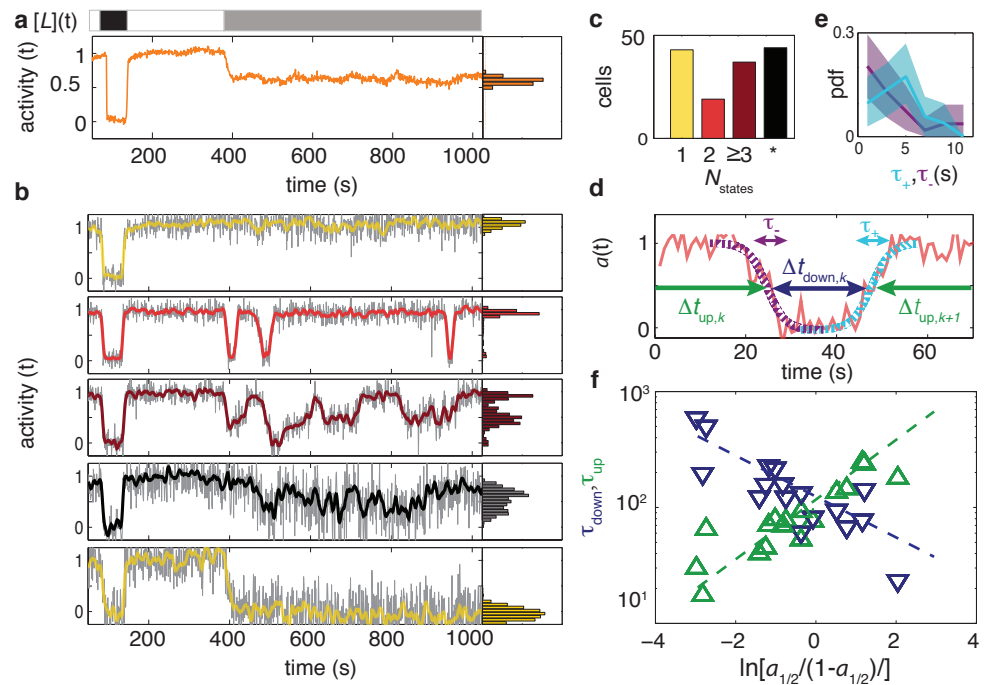
Figure 5. Temporal fluctuations in adaptation-deficient cells expressing Tsr as the sole chemoreceptor (TSS1964). **(a)** (Top) Step response protocol with L-serine. At the start of the experiment, a high (1mM) step response is applied for a rshort time (black). After flushing buffer for several minutes (white) a 20 μM step is applied for ±10 minutes (grey). (Middle) Population-averaged time series of 58 cells responding to the step response protocol. **(b)** Selected single-cell time series of the population shown in panel (a), each normalized to its baseline activity level before adding the first stimulus. To the unfiltered data (grey) a 7s moving average filter is applied and superimposed (colored according to categories in panel (c)). All time series and corresponding activity histograms of the same experiment are shown in Figure 5 - Supplement 1 and 5 - Supplement 2. **(c)** Categorization of the single-cell responses by the number of stable activity levels during the application of the stimulus near K of the population. Many cells show only one stable activity level (yellow), corresponding to either a full or none response. Some cells show two stable states (red) or more (purple). In other cells stable states did not show stable states (black). **(d)** Analysis on cells showing two-state switching to characterize transition times to and residence times in the stable states. Only two-state switchers are analysed in at least 75% of the activity level changed. Transition times t_+ and t_- are determined by fitting a sigmodial function (see main text) to the transient part of the time series. Residence times were defined as the interval between two successive transitions, at 50% activity. **(e)** Histogram of transition times, τ_+ (4.2 ± 2.2s, 26 events, cyan) and τ_- (3.5 ± 3.2, 29 events, purple) from in total 10 cells of a single experiment with 1 Hz acquisition frequency. **(f)** Residence times τ_{up} and τ_{down} as a function of the average activity level $a_{1/2}/(1 - a_{1/2})$. $a_{1/2}$ is defined as the fraction of time spend in the high activity state. The crossover point, obtained from linear fits of $a_{1/2}/(1 - a_{1/2})$ to $\log(\tau)$, is at 110 ± 10 and the slopes are $\gamma_{up} = 0.4 \pm 0.1$ and $\gamma_{down} = -0.6 \pm 0.1$. All fit results are ± the standard error from the fit. In total 17 cells are analyzed from 3 independent experiments (one at 1 Hz sampling, two at 0.2 Hz sampling).

Figure 5 - Supplement 1 All single-cell FRET time series from a single representative experiment.
Figure 5 - Supplement 2 Histograms of activity during attractant stimulus for all single cells from a representative single experiment.
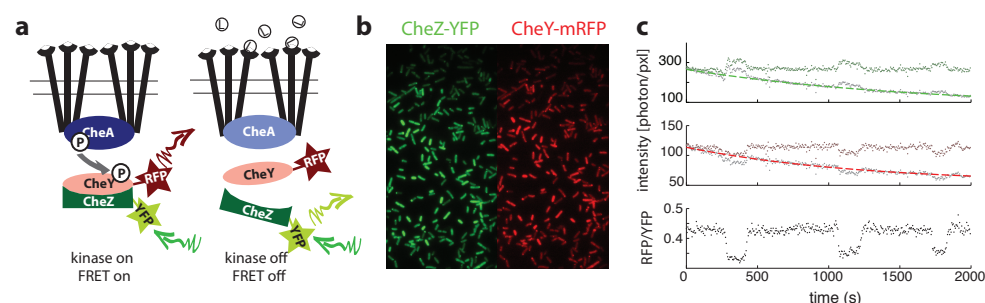
1092 **Supplemental Information**

Figure 1 - Supplement 1. Single-cell FRET assay schematic and workflow. **a)** Schematic of CheY-CheZ FRET assay. In absence of ligand stimuli, receptors are activating CheA. When active, CheA phosphorylates CheY, increasing interaction between CheY and phosphatase CheZ and thereby increasing FRET through the labeled fluorophores. Ligand-receptor binding shuts down the kinase, which ceases phosphate transfer and FRET levels decrease. **b)** False-color images of donor (CheZ-YFP) and acceptor (CheY-mRFP1) fluorescence, channels projected on the same EM-CCD camera chip. **c)** Example time series fluorescence from a single cell (CheRB-,VS149/pVS149/52). In grey raw data is shown, with a fit to a single exponential function with offset overlaid for donor (top, green) and acceptor channel (middle, red). From the corrected fluorescence intensities the ratio RFP/YFP is calculated (bottom).
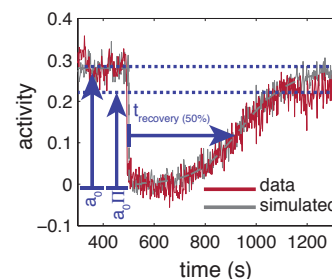
Figure 1 - Supplement 2. Influence of experimental noise on estimating recovery times. Simulated time series for are calculated by integrating the linearized MWC model with adaptation kinetics (*Tu et al., 2008*) with parameters chosen to closely approximate the population averaged response (grey-dashed line). To the simulated time series of each cell gaussian white noise ($\mu = 0; \sigma = 0.15$, 55 cells) is added to approximate the noise level of the experiment. Also shown are the baseline and recovery levels (blue dashed lines) of the experimental population.
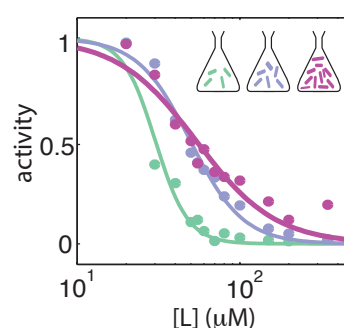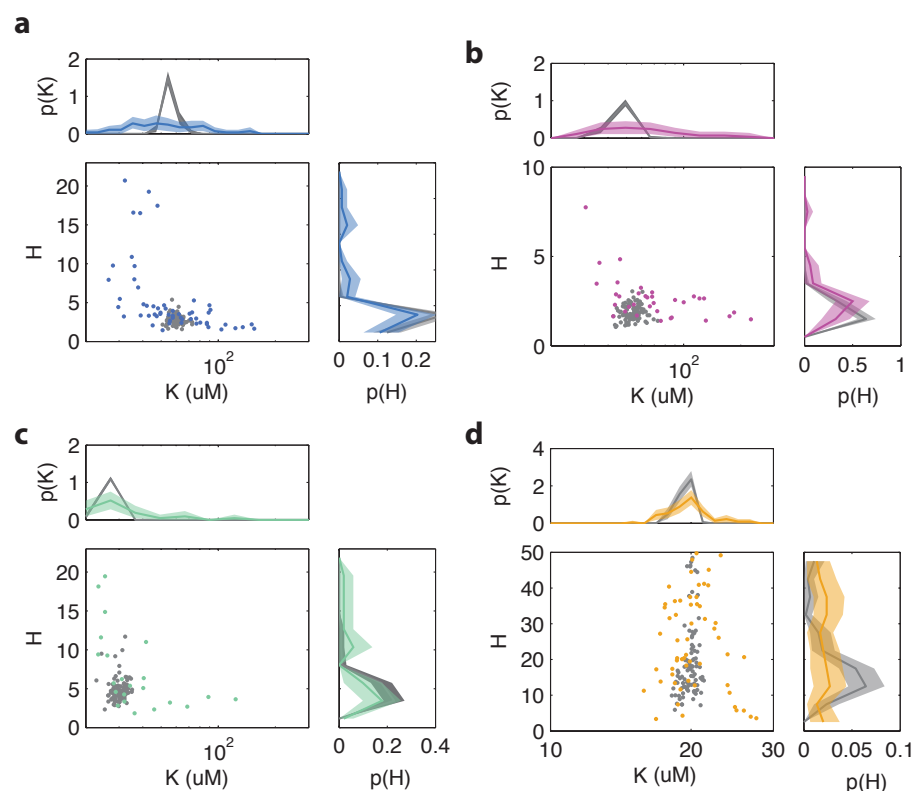

Figure 2 - Supplement 1. Dose response curves from population-averaged time series at harvesting OD's 0.31 (green), 0.45 (blue) and 0.59 (purple). The K/H fit value pairs are respectively 30/4.3, 50 /2.7 and 53/1.8.
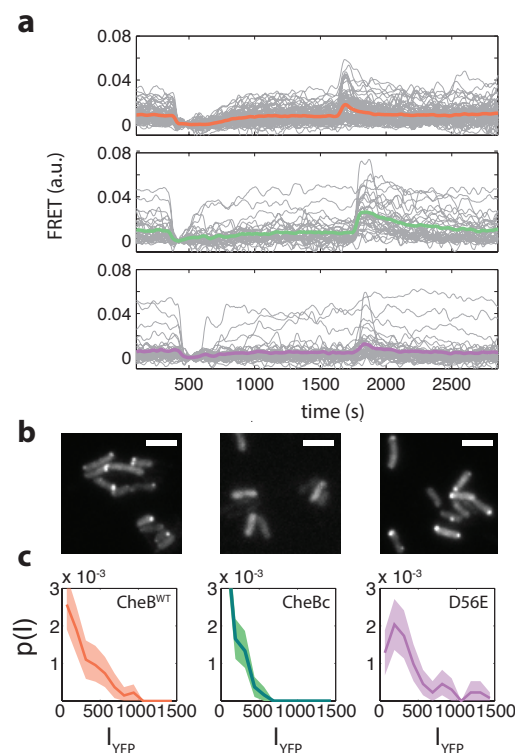
Figure 2 - Supplement 2. Influence of experimental noise on fit parameters K and H from Hill curve fits to single-cell dose-response experiment. Colored points and lines indicate fits to measurement data, gray lines and points are from a simulation in which gaussian white noise is added to a dose response curve with K and H obtained from a fit to the population averaged time series. The noise level of the simulation is chosen such to approximate the average mean-squared error [MSE] of the dose response curve fits. Experimental data with a MSE exceeding a determined threshold are removed from the analysis. For the experiment on cells with WT receptor complement (TSS58) a maximum mse of 0.05 is used, excluding 5 cells for **(b)** for the experiment at OD=0.45, this excludes 5 cells, at **(d)** OD=0.31, 3 cells and at **(c)** OD=0.59, 6 cells. **(d)** For the experiment on Tsr-WT (UU2567) 11 cells are removed by the same criterion. All shaded areas indicate 95 % confidence intervals obtained through bootstrapping.

Figure 3 - Supplement 1. a Example time FRET time series for cells expressing CheB^{WT} (top, pink), CheB^{D56E} (bottom,purple) , CheB$_c$ (middle, green) in ΔCheB (VS124) background. **b** Localization of CheB in the cell probed by mVenus fusions to CheB. Clustering was quantified by the fraction of cells clearly showing one or more clusters in the cell. Shown are representative examples of CheB^{WT} (left, 78% clustered), CheB$_c$ (middle, 0%), CheB^{D56E} (right, 72%). Scale bars 2 μm. **c** Histograms fluorescence intensity for single-cells in units of photons/pixel. Mean and standard deviation of these distributions for the strains is (from left to right) 272 ± 237 (114 cells), 148 ± 133 (150 cells) and 398 ± 328 (106 cells). This corresponds to CV 0.87, 0.90, 0.82 for the different CheB genotypes.
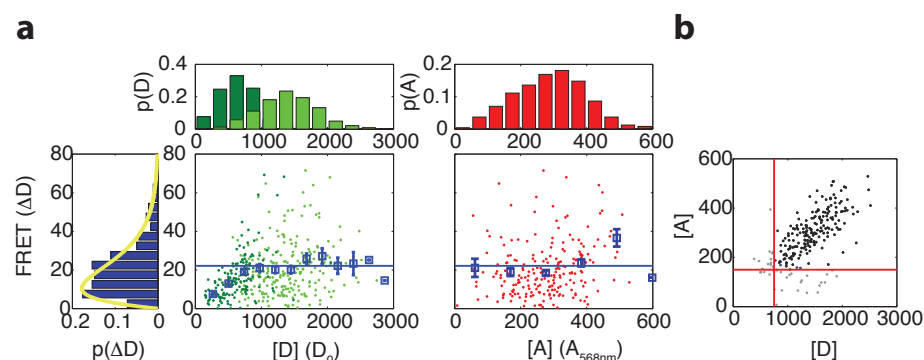
Figure 3 - Supplement 2. Relation between maximum FRET response and FRET fluorophore expression levels. **a)** (Left) Scatter plot with donor intensity (D_0, green) versus FRET response to 500 μM MeAsp (ΔD) and (right) acceptor intensity (A, red, measured by direct excitation) with marginal distributions for A, D and ΔD in VS104/pSJAB12. For the donor intensity we measured at low induction (10 μM IPTG, dark green) and high induction (100 μM IPTG, light green). The acceptor intensities were only measured at high induction. In the scatter plots the mean FRET response is plotted with the error bars (blue), the horizontal line indicating the average for the binned data as described in panel (b). The yellow curve is a fit to a gamma distribution with corresponding values and 95% confidence intervals of $k = 2.0 \pm 0.4$ and $\theta = 10.2 \pm 2.5$. All fluorescent intensities are measured in photons/pixel. All histograms are normalized to the number of cells. **b)** Gating of the data. Scatter plot of donor intensity versus acceptor intensity. All data with fluorescent intensities (in photons/pixel) lower than D=750 or A=175 are excluded from the analysis since the FRET response depends on donor and acceptor intensity levels below these levels. The distribution of the FRET response (extreme left) is only for the gated data.
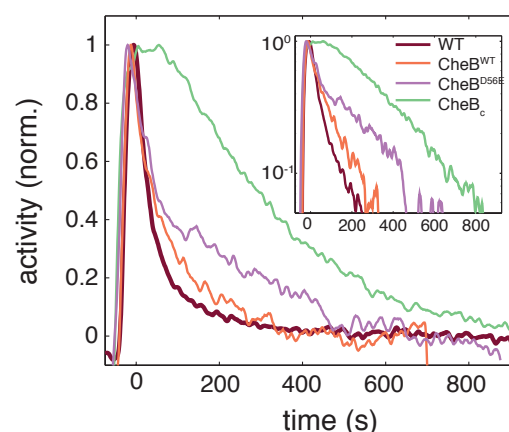
Figure 3 - Supplement 3. Phosphorylation feedback is not a necessary condition for fast removal adaptation dynamics. Population FRET time series of cells expressing CheB^{WT} (orange), CheB^{D56E} (purple) , CheB$_c$ (green) in ΔCheB (VS124) background as well as WT (CheB from native chromosome position, VS104, brown) are shown after removal of 500 μM to which cells have adapted. The strain expressing CheB^{D56E} lacks phosphorylation feedback but has a fast removal response. The population FRET experiment is performed as described previously (*Sourjik and Berg, 2002b*). The strains and induction levels are the same as in the single-cell FRET experiments on the CheB mutants.
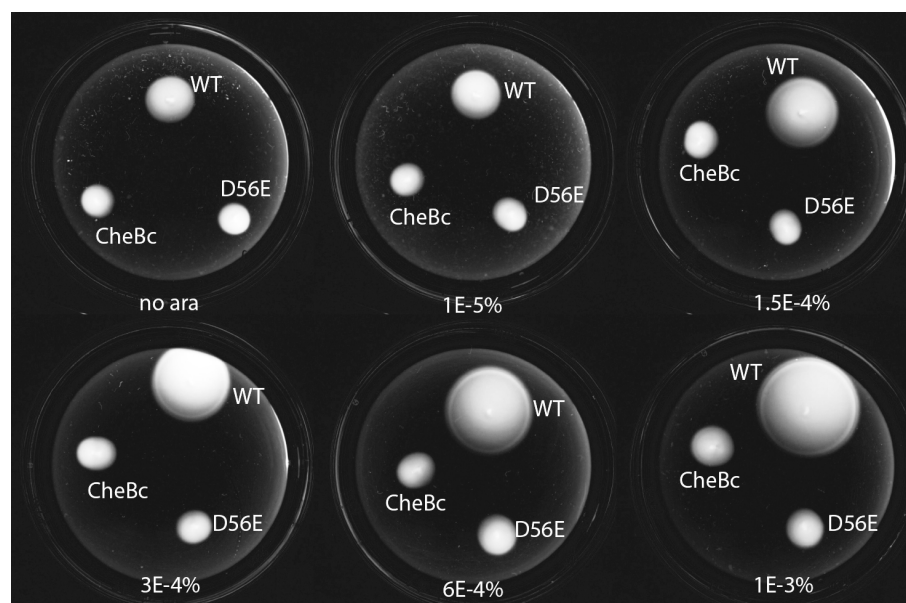
Figure 3 - Supplement 4. Phosphorylation defective mutants show impaired chemotaxis on soft agar. Dark-field images after 14 h of growth and motility on soft agar plates (0.26 % agar in TB with appropriate antibiotics, kept at 33.5 ^{o} C). The different strains express either WT CheB, CheB-D56E and CheBc from an arabinose inducable pBAD plasmid in Δ CheB strain (UU2614). The arabinose concentration is varied from 0 % to 0.001 %
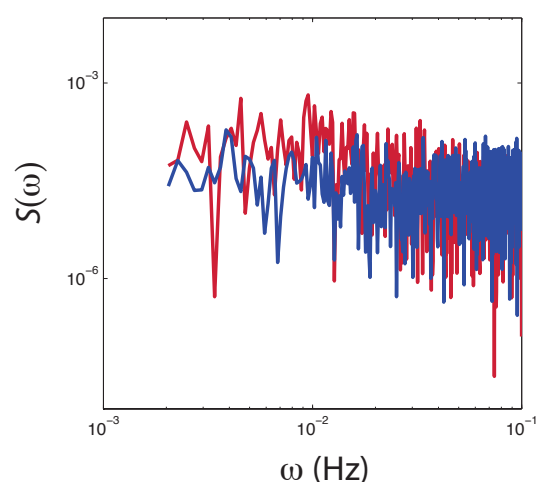
Figure 4 - Supplement 1. Power spectral density estimates from population averaged time series of CheRB+ (red) and CheRB- cells (blue). The time series are from the same experiment as shown in Figure 3b
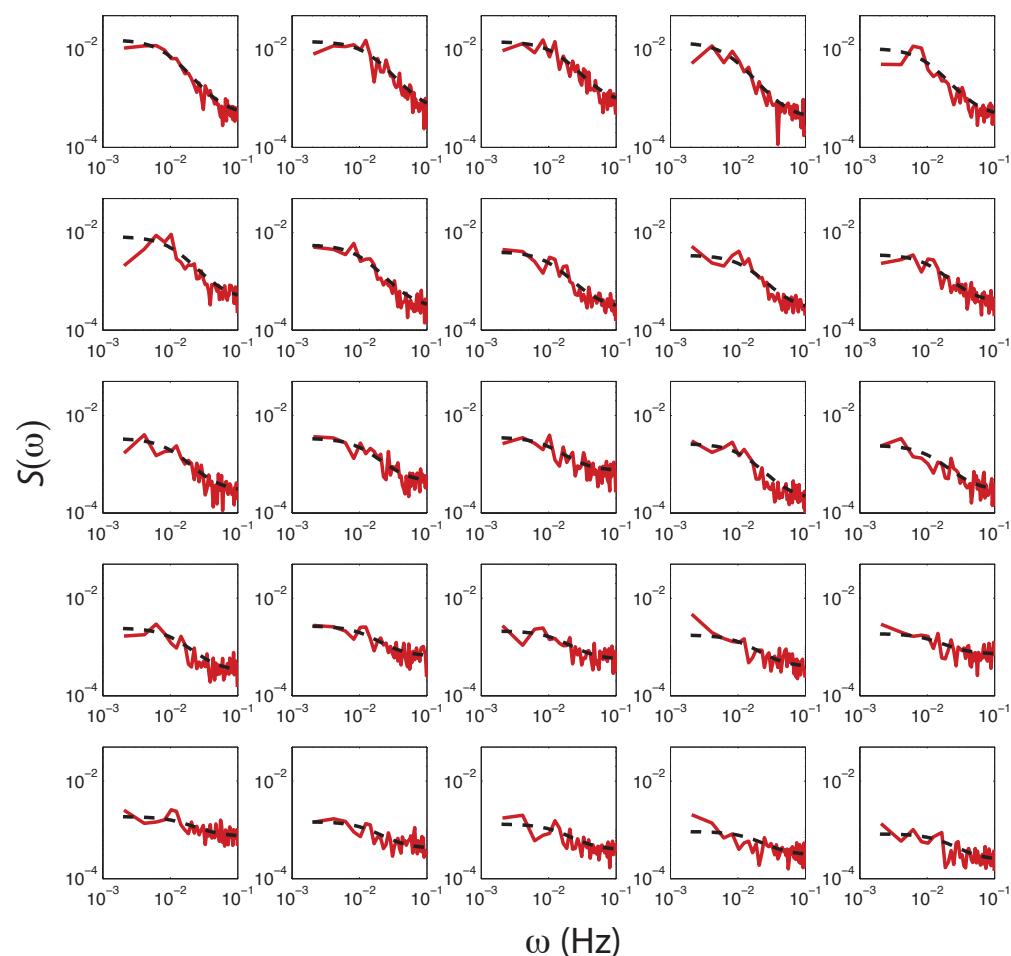
Figure 4 - Supplement 2. PSD estimates obtained from single-cell FRET time series (red dashed curve) with fits of O-U process to PSD estimates to 25 out of 31 cells (black dashed curve) from a single experiment shown in Figure 3b. The cells are sorted by variance calculated from the fit ($c\tau/2$), with top-left having the highest. Cells without a clear low frequency plateau, higher than five times the standard deviation of the high frequency noise, were excluded from the analysis.
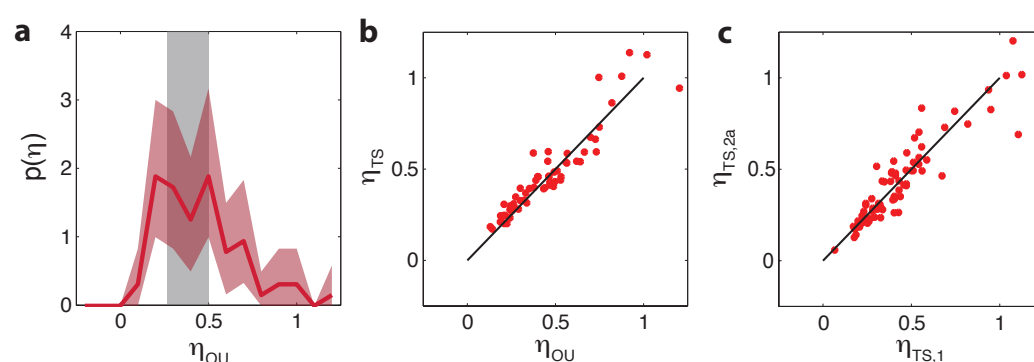
Figure 4 - Supplement 3. Comparison between noise amplitudes obtained from time series and power spectra. **a** Noise amplitude $\eta_{OU} = \sqrt{c\tau_m/2}/\langle a \rangle$ for 75 CheRB+ cells time series (from 3 experiments) obtained with mean noise level of 0.42. 14 cells without a clear low frequency noise plateau, at least five times the standard deviation of the high frequency noise floor of the power spectrum, were excluded from the analysis because τ could not be constrained by the fit. The grey shaded area indicates the expected noise amplitude variability based on a finite time window and experimental noise in the experiment (see Materials and Methods). The width is defined as the mean plus (minus) one standard deviation of the distribution of noise amplitudes obtained from simulated OU time series. **b** Noise amplitude η_{OU} obtained from fits of Ornstein-Uhlenbeck process to power spectra versus the noise amplitude η_{TS} obtained through calculating the standard deviation of the FRET time series after 10s average filtering. Also shown is the diagonal $\eta_{OU} = \eta_{TS}$. **c** The noise amplitude of the first ($\eta_{TS,1}$) and second half ($\eta_{TS,2}$) of the time series show high correlation, indicating that fluctuations are constant throughout the experiment. All noise amplitudes are defined as coefficient of variance.
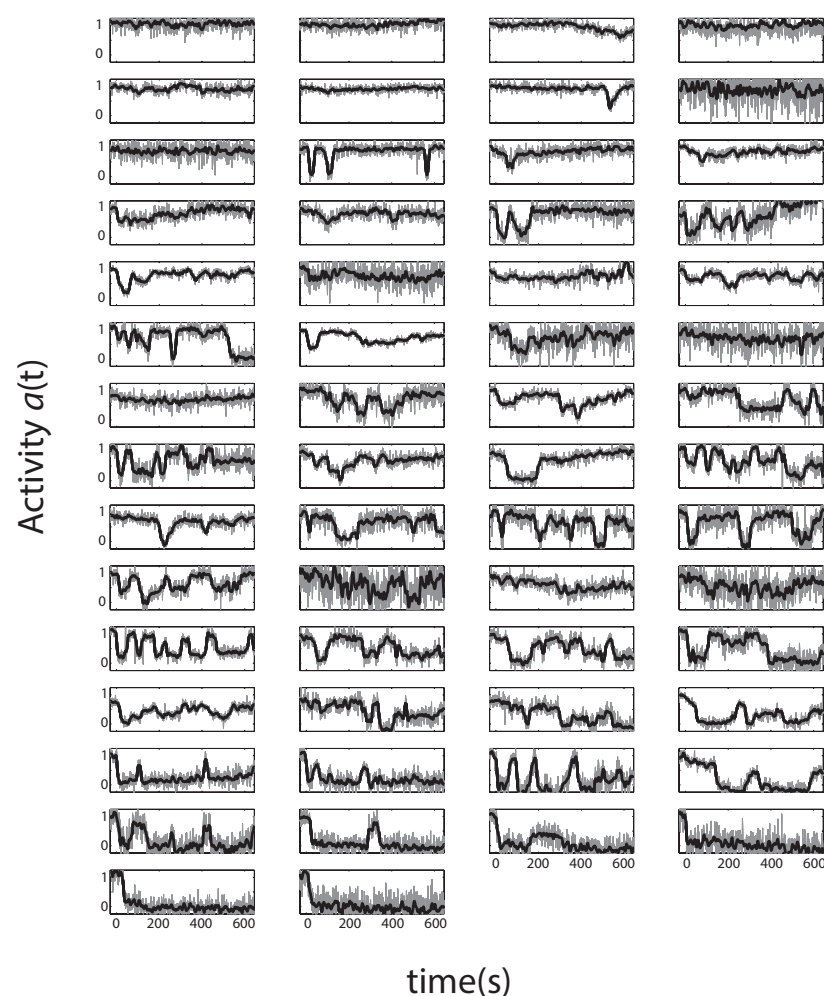
Figure 5 - Supplement 1. Single-cell activity time series from a step response FRET experiment. Shown are 58 cells with Tsr as the only chemoreceptor in CheRB- background (TSS1964) exposed to a step stimulus of 20 μM L-serine, each normalized to their own response amplitude. Time 0 is set to the time at which the population-averaged signal starts responding to a stimulus. The panels are ordered by the average activity level over the plot range.
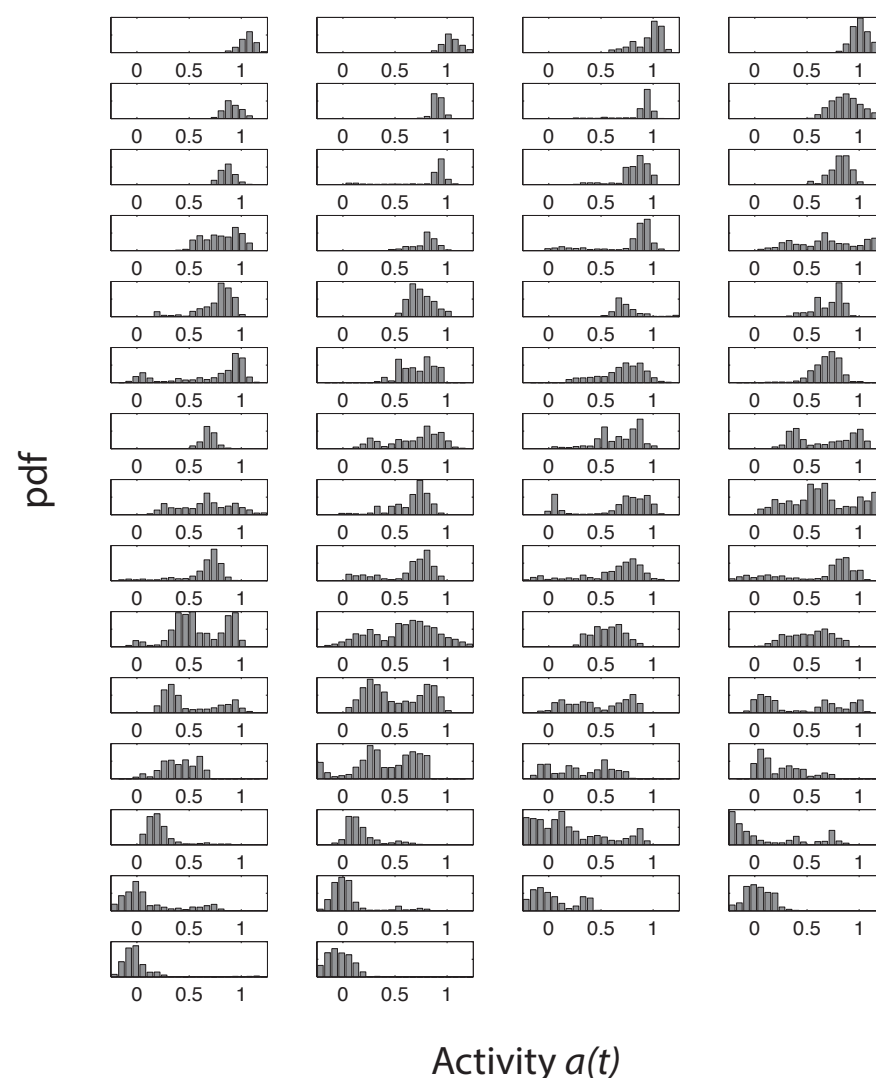
Figure 5 - Supplement 2. Single-cell activity histograms series from a step response FRET experiment. Shown are 58 cells with Tsr as the only chemoreceptor in CheRB- background (TSS1964) exposed to a step stimulus of 20 μM L-serine. The order of the plots is the same as in Figure 5 - Supplement 1